Displaced or invisible? ALPs from B decays at Belle II

T. Ferber,[1] **A. Filimonova,**[2] **R. Schäfer,**[3] **and S. Westhoff**[3]

[1]*Institute for Experimental Particle Physics, Karlsruhe Institute of Technology (KIT), 76131 Karlsruhe, Germany*

[2]*Nikhef, Science Park 105,1098 XG Amsterdam, The Netherlands*

[3]*Institute for Theoretical Physics, Heidelberg University, 69120 Heidelberg, Germany*

E-mail: torben.ferber@kit.edu, a.filimonova@nikhef.nl, r.schaefer@thphys.uni-heidelberg.de, westhoff@thphys.uni-heidelberg.de

ABSTRACT: At colliders, neutral long-lived particles can be detected through displaced decay products or as missing energy. Which search strategy is better depends on the particle's decay length just as on the detector properties. We investigate the complementarity of displaced and invisible signatures for the Belle II experiment. Focusing on axion-like particles a produced from meson decays, we present a new search strategy for two-body decays $B^+ \to K^+ a, a \to \not{E}$ with missing energy $\not{E}$. With $50\,\text{ab}^{-1}$ of data, Belle II can probe light invisible resonances with branching ratio $\mathcal{B}(B^+ \to K^+ a) \gtrsim 10^{-7}$ and decay length $c\tau_a \gtrsim 1\,\text{m}$. For axion-like particles, we expect the sensitivity of $B^+ \to K^+ \not{E}$ to small couplings to improve by up to two orders of magnitude compared to previous searches at collider and fixed-target experiments. For sub-GeV particles, $B^+ \to K^+ \not{E}$ at Belle II and searches at beam-dump experiments are most sensitive; for heavier particles, searches for displaced vertices at Belle II, long-lived particle experiments at the LHC, and future fixed-target experiments can probe the smallest couplings.

Contents

1 Introduction

The lifetime of a particle is a matter of fact; its detection is a matter of perspective. At colliders, a long-lived particle (LLP) may decay within the detector and leave traces of displaced decay products. Or it may traverse the detector and only be reconstructed as missing energy from the remainder of the event. In either case, the sensitivity depends on the particle's source and kinematics just as much as on the experimental setup and detector properties. To determine the discovery potential at an experiment, we have to consider case by case: Which search strategy is most sensitive - *displaced or invisible*?

Particle physics experiments are sensitive to LLPs within a huge range of masses and lifetimes [1, 2]. Collider experiments with a small detector coverage around the collision point, like LHCb [3] and FASER [4], mostly rely on displaced decays within the detector. Similarly, fixed-target experiments with a directional source are often designed to detect visible final states [5–7], but can also be sensitive to signatures with missing energy [8, 9]. At these experiments, the search strategy for LLPs is usually determined by the geometrical setup. On the other hand, collider experiments with a large detector coverage like ATLAS, CMS and Belle II can perform searches for both displaced vertices [10–12] and for missing energy [13–16]. Here the optimal search strategy is much less predictable, especially for particles with decay lengths that are comparable with the scales of the detector.

In this work we compare displaced and invisible signatures at the Belle II experiment. For concreteness, we focus on axion-like particles (ALPs) which can be resonantly produced in B meson decays. Belle II is perfectly suited to search for ALPs a in $B \to Ka, a \to \ell^+\ell^-$ decays with displaced leptons, as well as in $B \to K\!\!\!/\!\!\!E$ decays with missing energy. This versatility is mostly due to the large angular detector coverage and an excellent reconstruction efficiency for charged particles. Previously, BaBar has performed searches for light resonances X in $B \to KX, X \to \ell^+\ell^-$ with displaced leptons [17] and a search for a leptophilic scalar ϕ in $e^+e^- \to \tau^+\tau^-\phi, \phi \to \ell^+\ell^-$ with displaced leptons [18]. Belle has searched for long-lived heavy neutral leptons ν_h in $B \to X\ell\nu_h, \nu_h \to \ell^-\pi^+$ with displaced leptons and pions [19]. For Belle II, new searches with visible final states from LLP decays produced in B meson decays [20, 21] or directly from e^+e^- collisions [11, 12] have been proposed.

Searches for $B \to K\!\!\!/\!\!\!E$ with missing energy, on the contrary, have so far only been performed in the context of neutrinos in $B \to K\nu\bar{\nu}$ [16, 22, 23]. These analyses have been optimized for three-body decay kinematics, and some of them even reject two-body decays to suppress background.

We propose a new dedicated search strategy for invisible ALPs in two-body decays $B^+ \to K^+a, a \to \!\!\!/\!\!\!E$ at Belle II. To optimize the sensitivity, we perform a detailed analysis of the dominant background processes and identify selection criteria for a low-background region. With such a search, Belle II can probe ALPs with very small couplings that have not been explored in existing experiments. Our strategy can also be used more generally to search for light neutral scalars or pseudo-scalars produced from meson decays. To assess the complementarity of displaced and invisible searches, we compare our predictions for $B \to K\!\!\!/\!\!\!E$ with existing predictions for $B \to KX, X \to \ell^+\ell^-$ decays at Belle II [20].

This article is organized as follows. In Sec. 2, we introduce a model for the production and decay of long-lived ALPs in meson decays. In Sec. 3, we discuss existing bounds on the ALP parameter space from searches at flavor and fixed-target experiments. In Sec. 4, we present our new search strategy for invisible ALPs with $B \to K\!\!\!/\!\!\!E$ decays at Belle II and determine the projected sensitivity to light resonances. In Sec. 5, we compare these projections with the search potential for displaced $B \to Ka, a \to \ell^+\ell^-$ decays at Belle II. We conclude in Sec. 6 with an outlook on complementary ALP searches with displaced and invisible signatures at future experiments.

2 ALP model and benchmarks

Axion-like particles are new pseudo-scalars whose interactions with Standard Model (SM) particles preserve a global shift symmetry $a \to a + c$, where a is the ALP field and c is a constant. Originally, axions were proposed as a solution to the strong CP problem in QCD [24–27]. More generally, axion-like particles can be predicted in many theories with spontaneously broken symmetries as pseudo Nambu-Goldstone bosons. At colliders, light pseudo-scalars can be produced in rare meson decays $M_1 \to M_2\, a$ [28–34]. Meson

decays via flavor-changing neutral currents are suppressed in the Standard Model, but can be strongly enhanced if the ALP is resonantly produced. In this work, we are mostly concerned with $B \to Ka$ decays which probe ALPs with masses $m_a < m_B - m_K$. At energy scales μ above the weak scale, μ_w, the relevant ALP couplings are described by an effective Lagrangian [35][1]

$$\mathcal{L}_{\text{eff}}(\mu > \mu_w) = \sum_f \frac{c_{ff}(\mu)}{2} \frac{\partial^\mu a}{f_a} (\bar{f}\gamma_\mu\gamma_5 f) + c_{WW}(\mu) \frac{a}{f_a} \frac{\alpha_2}{4\pi} W^A_{\mu\nu} \widetilde{W}^{\mu\nu,A}. \qquad (2.1)$$

The ALP can be interpreted as the Goldstone boson of a spontaneously broken global chiral symmetry, broken at the cutoff scale $\Lambda = 4\pi f_a$ of the effective theory. In QCD, f_a is closely related to the axion decay constant. In our analysis we set $f_a = 1\,\text{TeV}$. Furthermore, c_{ff} denotes the ALP coupling to SM fermions f in the mass basis, and c_{WW} is the ALP coupling to the weak gauge bosons with field strength tensor $W^A_{\mu\nu}$, normalized to the weak coupling $\alpha_2 = g^2/4\pi$. We assume that at the cutoff scale the fermion couplings $c_{ff}(\Lambda)$ are flavor-universal and flavor-diagonal. Flavor diagonality implies that only flavor-conserving axial-vector couplings are physical. We do not consider ALP couplings to gluons or the hypercharge field in our analysis, assuming that they are not generated in UV completions at the TeV scale.

To make predictions for flavor observables, we evolve the coupling $c_{ff}(\Lambda)$ in (2.1) down to the bottom mass scale $\mu_b = m_b$ via the renormalization group (RG) [36–39].[2] To perform the RG evolution and matching at the weak scale $\mu_w = m_Z$, we have used a code [40] that is based on the results of Ref. [36]. The coupling c_{WW} is not renormalized and therefore constant above the weak scale.

The production rate for an ALP from $B \to Ka$ decays is

$$\Gamma_{B\to Ka} = \frac{\pi}{4} \frac{C_{sb}^2(m_b)}{\Lambda^2} f_0^2\left(m_a^2\right) m_B \left(1 - \frac{m_K^2}{m_B^2}\right)^2 \lambda^{1/2}(m_B^2, m_K^2, m_a^2), \qquad (2.2)$$

with the kinematic function $\lambda(a,b,c) = a^2 + b^2 + c^2 - 2(ab + ac + bc)$. The scalar form factor $f_0\left(m_a^2\right)$ parametrizes hadronic effects in $B \to K$ transitions at momentum transfer $q^2 = m_a^2$.[3] The Wilson coefficient C_{sb} describes the effective ALP interaction with left-handed bottom and strange quarks below the weak scale

$$\mathcal{L}_{\text{eff}}(\mu < \mu_w) \supset C_{sb}(\mu) \frac{\partial^\mu a}{f_a} (\bar{s}_L \gamma_\mu b_L) + h.c. \qquad (2.3)$$

The effective coupling is generated through loops of virtual top quarks and electroweak bosons. At the weak scale, it is well approximated by [36]

$$C_{sb}(\mu_w) = V_{ts}^* V_{tb} \left[(1 - R_t(\mu_w, \Lambda)) \, c_{tt}(\Lambda) \frac{\alpha_t}{4\pi} \left(\frac{1}{2} \ln \frac{\mu_w^2}{m_t^2} - \frac{1}{4} - \frac{3}{2} \frac{1 - x_t + \ln x_t}{(1 - x_t)^2} \right) \right. \qquad (2.4)$$

---

[1]We adopt the notation from Ref. [36], but express the fermion fields above and below the weak scale in terms of their mass eigenstates f.

[2]In general, the ALP couplings of left- and right-handed fermions evolve differently, with small effects on the flavor-diagonal couplings. For simplicity, we express the ALP-fermion couplings in terms of mass eigenstates f in (2.1), but include the full evolution in our numerical analysis.

[3]We implement the predictions for the scalar form factor from Ref. [41].

$$+ \frac{1}{9} R_t(\mu_w, \Lambda) \, c_{tt}(\Lambda) - c_{WW} \, \frac{\alpha_t}{4\pi} \frac{3\alpha}{2\pi s_w^2} \frac{1 - x_t + x_t \ln x_t}{(1 - x_t)^2} \Bigg],$$

where $\alpha_t = y_t^2 / 4\pi$ and $x_t = m_t^2 / m_W^2$. The function

$$R_t(\mu_w, \Lambda) \approx \frac{9}{2} \frac{\alpha_t(\mu_w)}{\alpha_s(\mu_w)} \left[1 - \left(\frac{\alpha_s(\Lambda)}{\alpha_s(\mu_w)} \right)^{\frac{1}{7}} \right] \tag{2.5}$$

describes the RG evolution of the ALP coupling to top quarks, c_{tt}, from the cutoff scale Λ down to the weak scale μ_w. Due to our assumption of flavor-universal ALP couplings c_{ff}, see (2.1), we identify $c_{tt}(\Lambda) = c_{ff}(\Lambda)$ in what follows. Below the weak scale, the RG evolution of C_{sb} is moderate, so that $C_{sb}(m_b) \approx C_{sb}(\mu_w)$.[4]

Expressed in terms of the three parameters c_{ff}, c_{WW} and m_a, the branching ratio for $B^+ \to K^+ a$ from (2.2) reads

$$\mathcal{B}(B^+ \to K^+ a) = 0.25 \left(c_{ff}(\Lambda) + 0.0032 \, c_{WW}(\Lambda) \right)^2 \frac{f_0^2(m_a^2)}{f_0^2(0)} \frac{\lambda^{1/2}(m_B^2, m_K^2, m_a^2)}{m_B^2 - m_K^2} . \tag{2.6}$$

The decay modes of the ALP vary strongly with the ALP mass. For $m_a < 2m_e$, the ALP can only decay into two photons at a rate

$$\Gamma_{a \to \gamma\gamma} = \frac{\alpha^2}{4\pi} \left| C_{\gamma\gamma}^{\text{eff}}(m_a) \right|^2 \frac{m_a^3}{\Lambda^2} , \tag{2.7}$$

with the effective coupling

$$C_{\gamma\gamma}^{\text{eff}}(\mu) \approx c_{WW}(\mu) + \mathcal{O}\left(\frac{\alpha}{4\pi} c_{ff} \right). \tag{2.8}$$

For $2m_e < m_a < 3m_\pi$, the ALP decays mostly into pairs of electrons or muons [36, 42],

$$\Gamma_{a \to \ell\bar{\ell}} = 2\pi m_a \frac{\left| C_{\ell\ell}^{\text{eff}}(m_a) \right|^2 m_\ell^2}{\Lambda^2} \sqrt{1 - \frac{4m_\ell^2}{m_a^2}} , \qquad \ell = \{e, \mu\} , \tag{2.9}$$

with the effective coupling[5]

$$C_{\ell\ell}^{\text{eff}}(\mu) = c_{ff}(\mu) + \mathcal{O}\left(\frac{\alpha^2}{16\pi^2} c_{WW} \right). \tag{2.10}$$

For masses $m_a > 3m_\pi$, the ALP can decay into hadrons. Below the scale of QCD confinement, the rate can be calculated in chiral perturbation theory; at high energies a perturbative treatment is possible. In the intermediate range around $\mu \approx 1\,\text{GeV}$, predictions of hadronic ALP decays are affected by large hadronic uncertainties and should be used with caution. For more details on our treatment of hadronic decays and a compendium of analytic expressions for all partial decay widths, we refer to App. A.

---

[4]In our numerical analysis we include RG effects below the weak scale.

[5]Even if fermion couplings are absent at the cutoff scale, $c_{ff}(\Lambda) = 0$, the ALP can still decay into leptons through loop effects of the gauge couplings. These decays are strongly suppressed by the electromagnetic coupling, they are not relevant for our analysis.
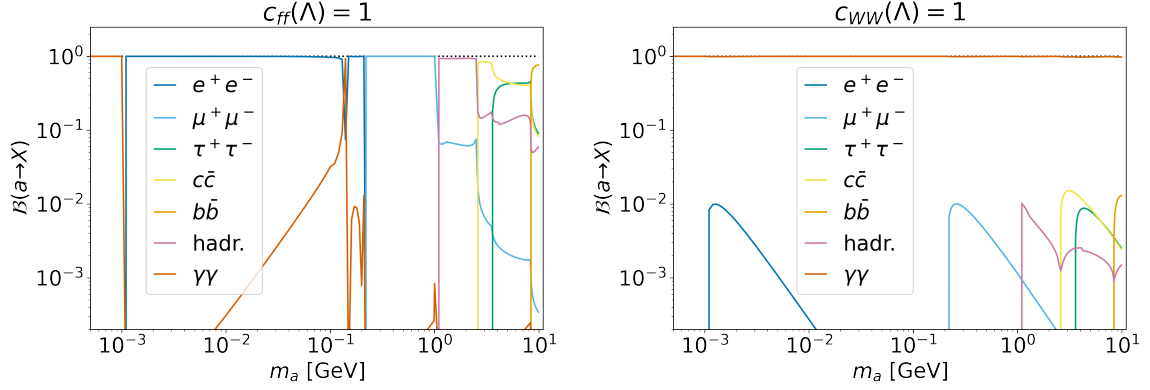
Figure 1: Branching ratios for ALP decays $a \to X$ in the c_{ff} scenario (left) and the c_{WW} scenario (right). The ALP couplings are fixed to $c_{ff}(\Lambda) = 1$ and $c_{WW}(\Lambda) = 1$ at the cutoff scale $\Lambda = 4\pi$ TeV.

Besides decays into SM particles, ALPs may also have exotic decay channels. In particular, an ALP could serve as a mediator to a dark sector and decay into invisible final states at a rate $\Gamma_{a\to\text{inv}}$. Assuming that no other decay channels exist, the total width of the ALP is given by

$$\Gamma_a = \Gamma_{a\to\gamma\gamma} + \sum_{\ell=e,\mu,\tau} \Gamma_{a\to\ell\bar\ell}\,\Theta(m_a - 2m_\ell) + \Gamma_{a\to\text{had}}\,\Theta(m_a - 3m_\pi) + \Gamma_{a\to\text{inv}}\,. \qquad (2.11)$$

The decay width of the ALP determines the lifetime $\tau_a = \Gamma_a^{-1}$. In our analysis, we focus on ALP decays into leptons and photons. Hadronic decays enter the phenomenology only through the lifetime.

For our analysis we define two benchmark scenarios:

$$\begin{aligned}
\text{``}c_{ff}\text{''}: &\quad \text{ALP coupling to fermions} &\quad c_{ff}(\Lambda) \neq 0,\ c_{WW}(\Lambda) = 0\,, &\qquad (2.12)\\
\text{``}c_{WW}\text{''}: &\quad \text{ALP coupling to gauge bosons} &\quad c_{WW}(\Lambda) \neq 0,\ c_{ff}(\Lambda) = 0\,.
\end{aligned}$$

The corresponding branching ratios of the ALP into the various final states are shown in Fig. 1. ALP decays to invisible final states are absent in these scenarios, so that $\Gamma_{a\to\text{inv}} = 0$ in (2.11).
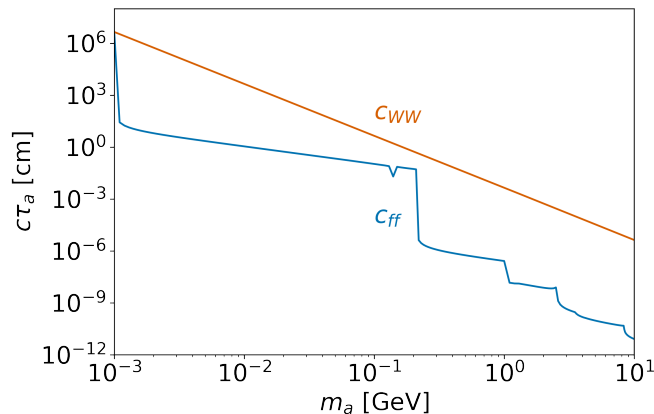
In the c_{ff} scenario, the partial decay rates of the ALP scale as

$$\Gamma_{a\to\ell\bar\ell} \propto c_{ff}^2(m_a)\,, \qquad \Gamma_{a\to\gamma\gamma} \propto \frac{\alpha}{4\pi}c_{ff}^2(m_a)\,. \qquad (2.13)$$

For masses $2m_e < m_a < 3m_\pi$, the ALP decays mostly into leptons. Decays into photons are loop-suppressed and dominate only for $m_a < 2m_e$.

In the c_{WW} scenario, the ALP decays according to

$$\Gamma_{a\to\ell\bar\ell} \propto \left(\frac{\alpha}{4\pi}\right)^4 c_{WW}^2(m_a), \qquad \Gamma_{a\to\gamma\gamma} \propto c_{WW}^2(m_a)\,. \qquad (2.14)$$

Figure 2: ALP decay length $c\tau_a$ as a function of the ALP mass m_a, for the two benchmark scenarios with $c_{ff}(\Lambda) = 1$ (blue) and $c_{WW}(\Lambda) = 1$ (orange) with $\Lambda = 4\pi$ TeV.

Here the ALP decays mostly into photons, while decays into leptons are loop-suppressed.

In Fig. 2, we display the proper decay length $c\tau_a$ of the ALP as a function of its mass m_a in the two benchmark scenarios with fixed couplings $c_{ff}(\Lambda) = 1$ and $c_{WW}(\Lambda) = 1$, respectively. In the c_{WW} scenario, the lifetime of the ALP is larger because ALP decays through gauge couplings are rare compared to decays through fermion couplings. For small ALP masses and/or small couplings, the decay length is macroscopic and the ALP tends to decay at a distance from the production point.

## 3 Bounds from flavor and fixed-target experiments

The search strategy for ALPs at flavor experiments depends on the lifetime and decay modes of the ALP. At short lifetimes, the ALP decays within the detector and may be observed in $B \to KX$ or $K \to \pi X$ decays with detectable final states $X = \{\mu^+\mu^-, e^+e^-, \gamma\gamma\}$. At long lifetimes, the ALP can be stable at detector scales and leave signatures with missing energy $\slashed{E}$, such as $B \to K\slashed{E}$ or $K \to \pi\slashed{E}$. For ALPs with intermediate lifetimes, it is a priori not clear whether searches with visible or invisible final states are most sensitive.

The expected event rate in the detector scales with the decay probability of the ALP. The probability to find an ALP with boost factor $\beta\gamma$ at a distance r from its production point is given by

$$\mathbb{P}_a(r|\beta\gamma) = \exp\left(-\frac{r}{d_a}\right), \qquad d_a = \beta\gamma c\tau_a, \tag{3.1}$$

where d_a is the ALP's decay length, defined in the laboratory frame. To obtain the average probability $\langle\mathbb{P}_a\rangle$ for an ALP to decay *outside* the detector in a sample of N events, we sum over all trajectories inside the detector volume and take into account the respective boost,

$$\langle\mathbb{P}_a\rangle = \frac{1}{N}\sum_{k=1}^{N}\mathbb{P}_a(r_k|\beta\gamma_k). \tag{3.2}$$
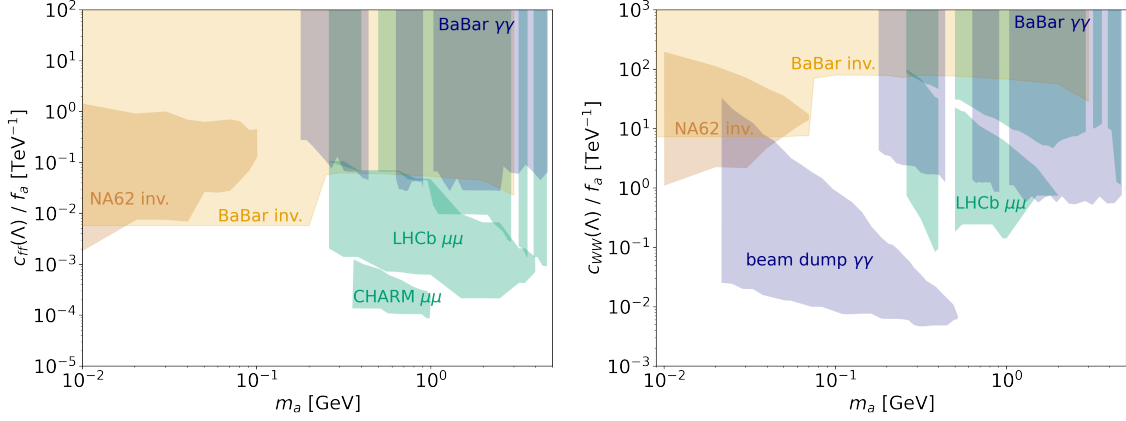
Figure 3: Bounds on the effective ALP coupling to fermions, $c_{ff}(\Lambda)/f_a$ (left), and weak gauge bosons, $c_{WW}(\Lambda)/f_a$ (right), as a function of the ALP mass m_a. Shown are bounds obtained from searches for $B^+ \to K^+ \nu \bar{\nu}$ at 90% CL by BaBar [22] (yellow), $K^+ \to \pi^+ \mu^+ \mu^-$ at 90% CL by NA62 [45] (orange), $B^+ \to K^+ \gamma \gamma$ at 90% by BaBar [44], for di-photon signals at 90% CL at the beam-dump experiments NuCal, CHARM and E137 [5] (blue), and searches for $B \to KX$, $X \to \mu^+ \mu^-$ with prompt and displaced muons at 95% CL by LHCb [43, 46] and CHARM [47] (green). Only one ALP coupling is present at $\Lambda = 4\pi$ TeV; all other couplings are set to zero.

Here r_k is the distance between the ALP production point and the point where it leaves the detector. If the ALP is produced in meson decays, the expected event rate for ALP decays inside the detector is given by

$$N_a(B \to KX) = N_B \, \mathcal{B}(B \to Ka) \times \mathcal{B}(a \to X) \times \left(1 - \langle \mathbb{P}_a \rangle\right), \tag{3.3}$$

where N_B is the number of B mesons produced in an experiment. For invisible ALPs, the event rate is

$$N_a(B \to K\!\!\!/E) = N_B \, \mathcal{B}(B \to Ka) \times \left(\mathcal{B}(a \to X) \times \langle \mathbb{P}_a \rangle + \mathcal{B}(a \to \text{inv})\right). \tag{3.4}$$

Here X refers to visible final states. Analogous expressions apply for $K \to \pi$ decays.

In this section we investigate the interplay of visible and invisible ALPs at flavor and fixed-target experiments. We derive bounds from existing searches for rare meson decays that can be interpreted in terms of ALPs. In Sec. 3.1, we focus on signatures with displaced leptons, most notably a search by LHCb for light resonances in $B \to K\mu^+\mu^-$ decays with displaced muon pairs [43]. In Sec. 3.2, we discuss signatures with photons in the final state, in particular the recent search for ALPs in $B \to K\gamma\gamma$ by BaBar [44]. In Sec. 3.3, we investigate searches with missing energy. We reinterpret a search for $B \to K\nu\bar{\nu}$ decays by BaBar [22] for invisible ALPs and derive bounds from a recent search for $K^+ \to \pi^+ X$, $X \to \text{inv}$ at NA62 [8, 9]. In Fig. 3 we summarize the strongest bounds on ALPs in the two benchmark scenarios from (2.12). All bounds apply for the effective ALP couplings $c_{ff}(\Lambda)$ and $c_{WW}(\Lambda)$ at the cutoff scale $\Lambda = 4\pi$ TeV. To derive these bounds from the measured observables, we

have RG-evolved the coupling $c_{ff}(\mu)$ in our predictions from $\mu = \Lambda$ down to the relevant scales for B and K decays, $\mu = m_b$ or $\mu = m_s$, as described in Sec. 2. The coupling $c_{WW} = c_{WW}(\Lambda)$ is constant above the weak scale and little affected by the RG evolution at lower scales.

3.1 ALP decays to leptons

ALPs that decay into leptons $\ell = \{e, \mu\}$ within the detector volume can be probed in $B \to K\ell^+\ell^-$ and $K \to \pi\ell^+\ell^-$ decays. The LHCb collaboration has performed searches for a light resonance X in $B \to KX$, $X \to \mu^+\mu^-$ decays with prompt [46] and displaced [43] muon pairs, as well as an inclusive search for di-muon vertices [48]. We reinterpret the search with displaced muons [43], which is most sensitive to ALPs with long decay lengths. Based on $3\,\text{fb}^{-1}$ of LHC data, LHCb has derived upper limits on the product of branching ratios, $\mathcal{B}(B^+ \to K^+X)\mathcal{B}(X \to \mu^+\mu^-)$. The results are reported for di-muon invariant masses in the range $250\,\text{MeV} < m_{\mu\mu} < 4700\,\text{MeV}$ and lifetimes of X ranging from 0.1 to 1000 ps. Our reinterpretation of these limits for ALPs with masses $m_a = m_{\mu\mu}$ is shown in Fig. 3. At the upper end of the excluded mass region (lower green area), $m_a \approx 1\,\text{GeV}$, the decay into muons is strongly suppressed by hadronic decays and the search loses sensitivity. The bounds on the coupling in the c_{ff} scenario (left panel) are stronger than in the c_{WW} scenario (right panel), due to the larger production rate (2.6) and branching ratio (2.14) into muons.

Larger ALP couplings are excluded by a similar search with less displaced di-muons (upper green area) [46], which is sensitive to ALPs with lifetimes $\tau_a < 0.2\,\text{s}$. A previous inclusive search for displaced vertices by BaBar [17] is not competitive with LHCb in the considered mass range [20].

Small couplings can also be constrained with the CHARM experiment. In Ref. [47], the authors have reinterpreted a search for sterile neutrinos at CHARM [49]. They report model-independent bounds on $\mathcal{B}(B^+ \to K^+X)\mathcal{B}(X \to \mu^+\mu^-)$ as a function of the lifetime τ_X for four fixed ALP masses. We interpolate between the provided mass benchmarks and show the resulting excluded regions in the ALP parameter space in Fig. 3 (green). The search is only sensitive to the c_{ff} scenario, where the ALP-lepton coupling is generated at tree level. In principle, CHARM could also search for lighter ALPs in $K \to \pi a, a \to \ell^+\ell^-$ decays. However, as explained in Ref. [50], most kaons are absorbed in the target, which drastically reduces the sensitivity to ALP decays in the far detector. We do not expect bounds from CHARM beyond the reach of missing energy searches at NA62 and BaBar, see Sec. 3.3.

ALPs with masses below the di-muon threshold can be probed with rare kaon decays. The NA48/2 experiment at CERN has measured the rare decays $K^+ \to \pi^+\mu^+\mu^-$ [45] and $K^+ \to \pi^+e^+e^-$ [51]. The measurement focuses on the SM topology, selecting three-track vertices from kaon decays. Due to this selection criterion the measurement cannot be reinterpreted for ALPs with long decay lengths, where the pion and di-lepton momenta do not point back to the same vertex. For ALPs with short decay lengths, the parameter region

for $m_a > 2m_\mu$ has been excluded by LHCb [46]. For lighter ALPs with large couplings, $K^+ \to \pi^+ e^+ e^-$ can set bounds in the range $140\,\text{MeV} < m_a < 354\,\text{MeV}$. In Sec. 3.3, we will see that this parameter region has been excluded by a recent search for $K^+ \to \pi^+ \not{E}$ at NA62 [8]. We therefore do not attempt to reinterpret the $K^+ \to \pi^+ \ell^+ \ell^-$ measurements.

3.2 ALP decays to photons

While ALP signatures with leptons mostly probe the fermion coupling c_{ff}, final-state photons are sensitive to the gauge coupling c_{WW}. Here we derive bounds on c_{WW} from searches for ALPs with photons at colliders and fixed-target experiments; for previous similar analyses see for instance Refs. [5, 52].

Recently the BaBar collaboration has performed a dedicated search for ALPs in $B^+ \to K^+ \gamma\gamma$ decays [44]. They report direct bounds on $\mathcal{B}(B^+ \to K^+ a)\mathcal{B}(a \to \gamma\gamma)$ for ALPs with masses of $175\,\text{MeV} < m_a < 4.78\,\text{GeV}$ and decay lengths $c\tau_a < 1\,\text{mm}$, and for $175\,\text{MeV} < m_a < 2.5\,\text{GeV}$ for longer decay lengths up to $c\tau_a = 100\,\text{mm}$. We show the resulting bounds in blue in Fig. 3.

In Fig. 3, we show the resulting bounds in the two ALP scenarios (blue area). In the c_{WW} scenario, the ALP decays to photons at tree level and the search by BaBar is very sensitive to small couplings. The bound is determined by the decreasing production rate, $\mathcal{B}(B^+ \to K^+ a) \sim c_{WW}^2$, except for small ALP masses, where the decay length exceeds $c\tau_a = 100\,\text{mm}$. In the c_{ff} scenario, the ALP decay into photons is loop-induced. The branching ratio $\mathcal{B}(a \to \gamma\gamma)$ is strongly suppressed, see (2.13), because the decay length of the ALP is dominated by the decay into fermions. The bounds on c_{ff} are therefore relatively weak and the sensitivity is limited by the rate, rather than the lifetime, except for the smallest accessible ALP masses. Nevertheless, it is remarkable that a photon search is sensitive to ALP couplings to fermions through quantum effects alone.

Searches for rare kaon decays are sensitive to ALPs with smaller masses. The fixed-target experiment E949 has searched for $K^+ \to \pi^+ \gamma\gamma$ decays in a phase-space region corresponding to di-photon invariant masses $m_{\gamma\gamma} < 108\,\text{MeV}$ [53]. The search targets the three-body decay topology; kinematic selections have been applied to reduce background, which limit the sensitivity to two-body kaon decays. Due to the lack of information on these selections and knowing that NA62's $K^+ \to \pi^+ \not{E}$ search (see Sec. 3.3) is more sensitive to long-lived ALPs, we do not attempt to reinterpret the E949 analysis.

At $e^+ e^-$ colliders, searches for di-photon resonances from direct ALP production via $e^+ e^- \to \gamma a$, $a \to \gamma\gamma$ are an interesting alternative to meson decays. The Belle II collaboration has performed such a search and derived bounds on the ALP coupling to photons for masses $200\,\text{MeV} < m_a < 9.7\,\text{GeV}$ [54]. With the current sensitivity, the reach is comparable with similar searches at LEP II and ATLAS [55], but is expected to improve with more data.

Long-baseline experiments are sensitive to ALPs with even smaller couplings, because the predicted production rate is high and the long baseline allows to probe long decay lengths.

The currently strongest bounds on the ALP-photon coupling arise from a combination of the proton beam-dump experiments NuCal, CHARM and E137 [5]. ALPs can be produced from bremsstrahlung photons[6] or via Primakoff conversion in the target, $\gamma Z \to aZ$.

For NuCal, CHARM and E137, we interpret the bounds from Ref. [5] in the c_{WW} scenario. The bound cannot be directly translated to the c_{ff} scenario; however, due to loop-suppressed ALP decays to photons we expect a lower sensitivity than in missing energy searches at BaBar and NA62. In Fig. 3, we see that NuCal, CHARM and E137 probe ALPs with masses $m_a \lesssim 500\,\text{MeV}$; the lower cutoff at $m_a = 200\,\text{MeV}$ was set by the experimental analysis. In the excluded region the decay length of the ALP matches the baseline and beam energy of the experiments. For the electron beam experiment NA64, we have checked that the bounds on c_{WW}/f_a obtained for $m_a \lesssim 60\,\text{MeV}$ by the collaboration in Ref. [7] do not exceed the reach of $B \to K \not{E}$ at BaBar.

3.3 Invisible ALP decays

ALPs that escape the detector can be caught in signatures with missing energy, notably in the rare meson decays $B \to K \not{E}$ and $K \to \pi \not{E}$.

Both BaBar [22] and Belle [23] have searched for the rare decays $B \to K^{(*)} \nu\bar{\nu}$ with SM neutrinos in the final state. The analysis by Belle has been optimized for three-body final states, explicitly removing events with two-body decay kinematics. The search is therefore insensitive to ALPs produced in $B \to Ka$ decays.

BaBar's search for $B \to K\nu\bar{\nu}$ [22] reports differential distributions of the momentum transfer $s_B = q^2/m_B^2$ in $B \to K$ transitions, which allows us to derive bounds on invisible ALPs produced via $B \to Ka$. The analysis employs hadronic B tagging, so that the $B \to K \not{E}$ decay kinematics can be fully reconstructed. The results based on $N_{B\bar{B}} = 471 \times 10^6$ $B\bar{B}$ pairs produced at the $\Upsilon(4S)$ resonance are presented in bins of width $\Delta s_B = 0.1$. We reinterpret the results from charged $B^+ \to K^+$ decays, which yield the strongest bounds. An ALP with mass m_a would increase the event rate $\Delta\mathcal{B}$ in the bin containing $s_B = m_a^2/m_B^2$ by

$$\Delta\mathcal{B}_a = \frac{\Delta N_a(B^+ \to K^+ \not{E})}{0.514\,N_{B\bar{B}}}\,, \tag{3.5}$$

with $N_a(B \to K \not{E})$ from (3.4). The factor 0.514 accounts for the different production rates of B^+ and B^0 mesons in the $B\bar{B}$ sample. We require the sum of ALPs and neutrinos to fall within $1.64\,\sigma$ of the observed event rate in this bin,[7]

$$\Delta\mathcal{B}\left(B^+ \to K^+ \nu\bar{\nu}\right) + \Delta\mathcal{B}_a \leq (1 + 1.64\sigma)\,\Delta\mathcal{B}\left(B^+ \to K^+ \not{E}\right)\,, \tag{3.6}$$

which corresponds to a confidence level of $90\,\%$ assuming Gaussian uncertainties. The neutrino background is very small, $\Delta\mathcal{B}\left(B^+ \to K^+ \nu\bar{\nu}\right) = 7.3 \cdot 10^{-7}$ for $s_B < 0.1$, which

---

[6]At proton beam dumps, another source of photons are meson decays.

[7]We have verified that the detector acceptance for kaons from $B \to K\nu\bar{\nu}$ and from $B \to Ka$ decays is nearly identical and does not affect the interpretation.

corresponds to $m_a \lesssim 1.6\,\mathrm{GeV}$. The resulting bounds on our ALP benchmarks are shown in Fig. 3 (yellow area).

The bounds on the ALP coupling in the c_{ff} scenario are generally stronger than in the c_{WW} scenario, due to the different production rates $\mathcal{B}(B \to Ka)$, see (2.6). The variation of the bounds with the ALP mass m_a is related to its decay length. For small masses, the ALP has a macroscopic decay length, see Fig. 2, and decays mostly outside the detector. In this region the search for $B^+ \to K^+a, a \to \not{E}$ is most effective. For larger masses, the ALP tends to decay close to its production point. Here the sensitivity is set by the detector acceptance, i.e., by the probability for the ALP decay products to miss the detector region. In either regime, the sensitivity is largely insensitive to the ALP mass. The small dip around $m_a \gtrsim 1.6\,\mathrm{GeV}$ is due to a slightly higher experimental sensitivity of BaBar for $s_B > 0.1$.

The sensitivity jump between light and heavy ALPs is explained by the interplay of production rate and decay length: When decreasing the coupling c/f_a of an ALP with a fixed mass, the production rate decreases as $\mathcal{B}(B \to Ka) \sim (c/f_a)^2$, while the probability not to decay inside the detector increases as $\exp(-(c/f_a)^{-2})$. The compensation of these two effects is very sensitive to the coupling, which explains the height of the sensitivity jump. In the c_{ff} scenario, the jump occurs close to the muon threshold $m_a \approx 2m_\mu$, where the ALP decay length decreases abruptly as the decay into muons opens. Searches for $K^+ \to \pi^+ \not{E}$ decays are sensitive to invisible ALPs with masses $m_a < m_K - m_\pi$. We calculate the branching ratio for $K^+ \to \pi^+ a$ in analogy to $B^+ \to K^+ a$ in Sec. 2 and obtain

$$\mathcal{B}(K^+ \to \pi^+ a) = 1.03 \times 10^{-4} \left(c_{ff}(\Lambda) + 0.0032\, c_{WW}(\Lambda) \right)^2 \frac{\lambda^{1/2}(m_K^2, m_\pi^2, m_a^2)}{m_K^2 - m_\pi^2}, \qquad (3.7)$$

where $c_{ff}(\Lambda) = c_{tt}(\Lambda)$, as in (2.6). The scalar form factor $f_0^K(q^2)$ has been computed in lattice QCD [56]. For simplicity, we set $f_0^K(q^2) = 1$ in our analysis, which slightly overestimates the ALP production rate. For the normalization at the kinematic endpoint, we use $|V_{us}| f_0^K(0) = 0.216$ [57], exploiting the relation $f_+^K(0) = f_0^K(0)$.

At the NA62 experiment, kaons are produced from a high-energetic proton beam impinging on a beryllium target. The decay products can be observed in a $60\,\mathrm{m}$ long fiducial volume. Recently the collaboration has interpreted their measurement of $K^+ \to \pi^+ \nu \bar{\nu}$ decays for two-body decays $K^+ \to \pi^+ X$ with a long-lived new particle X [8, 9]. They report limits on the branching ratio $\mathcal{B}(K^+ \to \pi^+ X)$ as a function of the X's mass for lifetimes $\tau_X > 100\,\mathrm{ps}$. We show the reinterpreted bounds in Fig. 3 (orange area). In the c_{WW} scenario, $K^+ \to \pi^+ \not{E}$ at NA62 is up to an order of magnitude more sensitive to small ALP couplings than $B^+ \to K^+ \nu \bar{\nu}$ at BaBar. In the c_{ff} scenario, NA62's sensitivity is comparable with BaBar only for small masses, because the ALP decay length is shorter than in the c_{WW} scenario.

NA62's measurement of $K^+ \to \pi^+ \nu \bar{\nu}$ is not sensitive to ALPs with masses $m_a \approx m_{\pi^0}$, due to a large background from $K^+ \to \pi^+ \pi^0$ decays. This region has been explored by NA62 in a dedicated analysis of invisible π^0 decays, which has been reinterpreted for $K^+ \to \pi^+ X$ decays with $\tau_X > 100\,\mathrm{ps}$ [58]. The resulting bounds are shown in Fig. 3 (yellow).

The KOTO experiment has searched for invisible particles X in $K_L^0 \to \pi^0 X$ decays [59]. However, KOTO's bound on $\mathcal{B}(K_L^0 \to \pi^0 X)$ assumes that all particles X are invisible in the experiment. An interpretation of the analysis for ALPs with a finite decay width would require a dedicated simulation and recast, which goes beyond the scope and purpose of this work.

Existing searches for visible and invisible ALP signatures complement each other in their sensitivity. For masses below the di-muon threshold, searches with missing energy at BaBar and NA62, as well as displaced photons at beam dumps lead the sensitivity to small ALP couplings. For heavier ALPs, searches for displaced di-muons at LHCb and CHARM, and a new search with displaced photons by Belle II dominate the bounds. Taken together, current searches set mass-dependent upper bounds on the ALP couplings

$$c_{ff}(\Lambda)/f_a \lesssim (10^{-3} - 10^{-2})\,\mathrm{TeV}^{-1}, \qquad c_{WW}(\Lambda)/f_a \lesssim (10^{-2} - 1)\,\mathrm{TeV}^{-1}\,, \qquad (3.8)$$

up to a few gaps in the parameter space, see Fig. 3. In what follows, we will explore the potential of Belle II to improve the sensitivity to long-lived ALPs with searches for missing energy or displaced vertices.

4 Search strategy for invisible ALPs at Belle II

The search for $B^+ \to K^+ a, a \to \not{E}$ is experimentally similar to the search for the SM process $B^+ \to K^+ \nu\bar{\nu}$, where Belle II recently pioneered an inclusive tagging approach to increase the signal efficiency [16]. This approach is in contrast with the exclusive method, where one B meson is completely reconstructed in a hadronic final state before reconstructing the signal-side B meson in the rest of the event [22]. In the text, we only refer to $B^+ \to K^+ a$ decays; charge-conjugate channels are implied in what follows. In contrast to $B^+ \to K^+ \nu\bar{\nu}$, $B^+ \to K^+ a$ is a two-body decay with very specific event kinematics. The signal hence consists of a single charged kaon that can be reconstructed in the tracking detectors, and missing momentum. Final states with neutral kaons could be included in a future analysis.

We study the Belle II sensitivity for a dataset corresponding to an integrated luminosity of 0.5 ab^{-1}, roughly equivalent to the full BaBar dataset, and a luminosity of 50 ab^{-1}, corresponding to the expected final dataset of Belle II. We generate events using the Belle II Analysis Software Framework [60, 61]. We do not simulate the detector response, but approximate efficiencies and acceptance as explained below. We expect the effect of such simplifications on triggers and resolution to be rather small. We also do not include effects of beam-induced backgrounds, which however will reduce the missing energy resolution in the real experiment.

4.1 Signal and background simulation

We generate the events in the e^+e^- centre-of-mass frame with the nominal Belle II collision energy of $\sqrt{s} = 10.58\,\mathrm{GeV}$, then boost and rotate them to the Belle II laboratory frame. The Belle II beam parameters are $E(\mathrm{e}^+) = 4.002\,\mathrm{GeV}$ and $E(\mathrm{e}^-) = 7.004\,\mathrm{GeV}$ with a 41.5 mrad crossing angle between the beams and the z-axis. In the laboratory frame the

z-axis is oriented along the bisector of the angle between the direction of the electron beam and the reverse direction of the positron beam. All selections below refer to parameters in the lab frame unless noted otherwise.

To produce signal events we generate events for $\Upsilon(4S) \to B^+B^-$, followed by decays of one B through $B^+ \to K^+a$ and the other B decaying generically. The decays of the charged B mesons are simulated using the EvtGen generator [62]: The signal-side B meson decay is using the EvtGen phase space model PHSP, while the generic B meson decay is using all available B meson decay modes of the Belle II decay descriptions. For each ALP mass benchmark we generate 10k events.[8]

To produce background events we generate $\Upsilon(4S) \to B^+B^-$ and $\Upsilon(4S) \to B^0\bar{B}^0$ using EvtGen. In addition we generate continuum backgrounds from $e^+e^- \to u\bar{u}(\gamma)$, $d\bar{d}(\gamma)$, $s\bar{s}(\gamma)$, $c\bar{c}(\gamma)$, using KKMC [63], simulate the hadronization of the quarks with PYTHIA8.2 [64], and model the decays of generated mesons with EvtGen. We also include background from $e^+e^- \to \tau^+\tau^-$, using KKMC and TAUOLA to generate and decay the tau leptons [65]. For each background channel, we generate 10 million events and use the following cross sections [66] to normalize their rates: 1.61 nb ($u\bar{u}$), 0.40 nb ($d\bar{d}$), 0.38 nb ($s\bar{s}$), 1.30 nb ($c\bar{c}$), 0.919 nb ($\tau\bar{\tau}$), 0.54 nb (B^+B^-), and 0.51 nb ($B^0\bar{B}^0$).

For our analysis we only consider final-state charged particles (e, μ, π, K, p) with transverse momenta $p_T > 0.2$ GeV and photons with energies $E > 0.05$ GeV. For both charged particles and photons, we require that they are in the acceptance of the central drift chamber of Belle II with polar angles $17° < \theta < 150°$. Neutrons, K_L^0, and neutrinos are counted as invisible. Short-lived resonances like K_S^0 and π^0 are decayed promptly and are included via their final-state decay products. We do not simulate the detector response for the generated particles, but we include an 80 % kaon identification efficiency and a 5 % pion misidentification rate [67] for both signal and background. In addition, we assume a track-finding efficiency of 99 % [68] per charged particle, and we approximate the photon detection efficiency with 100 %. We assume normal distributions for the relative momentum resolution of charged particles, $\Delta p/p = 0.5$ % [69], and for the relative energy resolutions for photons, $\Delta E/E = 5$ % [66].

4.2 Event selection

Signal B meson candidates contain one reconstructed kaon and missing momentum. All remaining final-state charged particles and photons are hence associated with the decay of the tag-side B meson. We reconstruct a missing-momentum vector $p_{\text{miss}} = (E_{\text{miss}}, \vec{p}_{\text{miss}})$, defined as the total momentum needed to balance the sum of momenta of all detected charged particles and photons, and the well-known initial state in the e^+e^- collision.

---

[8]We have simulated 12 ALP benchmarks with the masses $m_a = $ 5 MeV, 50 MeV, 70 MeV, 100 MeV, 200 MeV, 250 MeV, 300 MeV, 500 MeV, 1 GeV, 2 GeV, 3 GeV, and 4 GeV. For clarity, we only show 4 representative masses in Fig. 4, but we use all benchmark masses for constructing the bounds in Fig. 10 and 11.
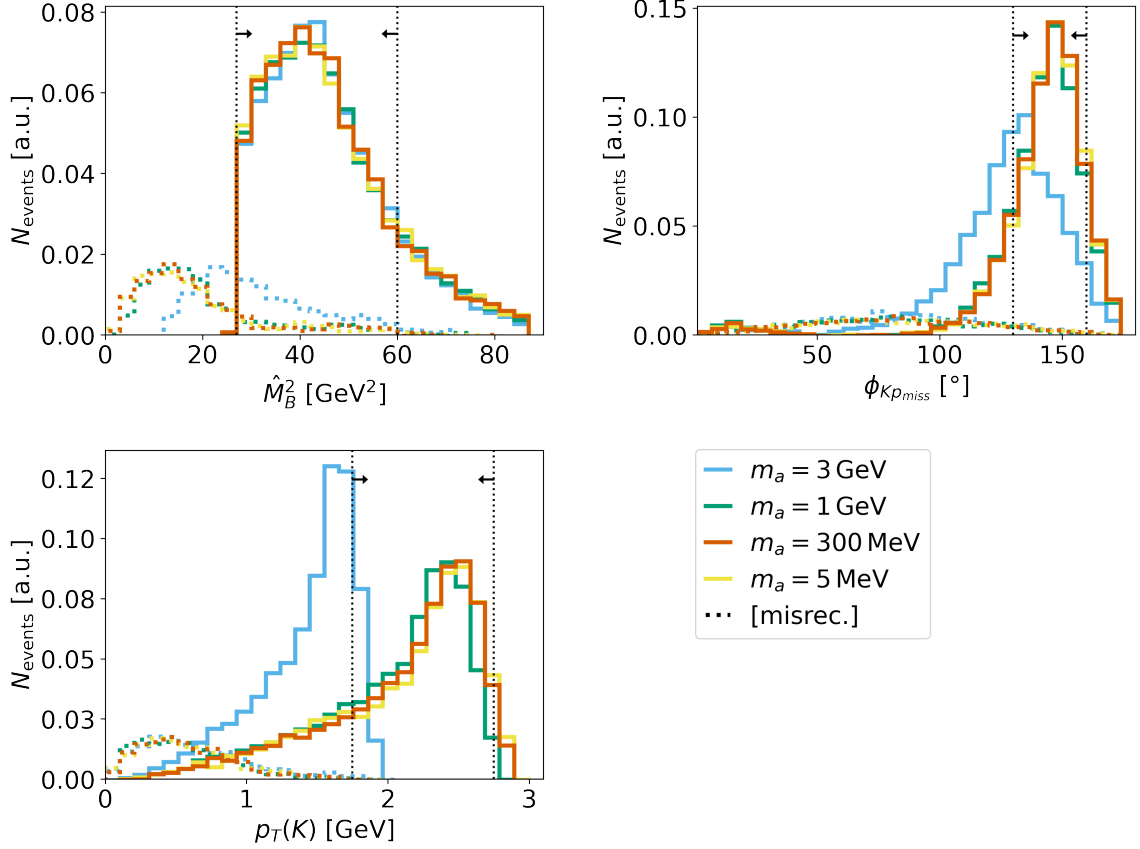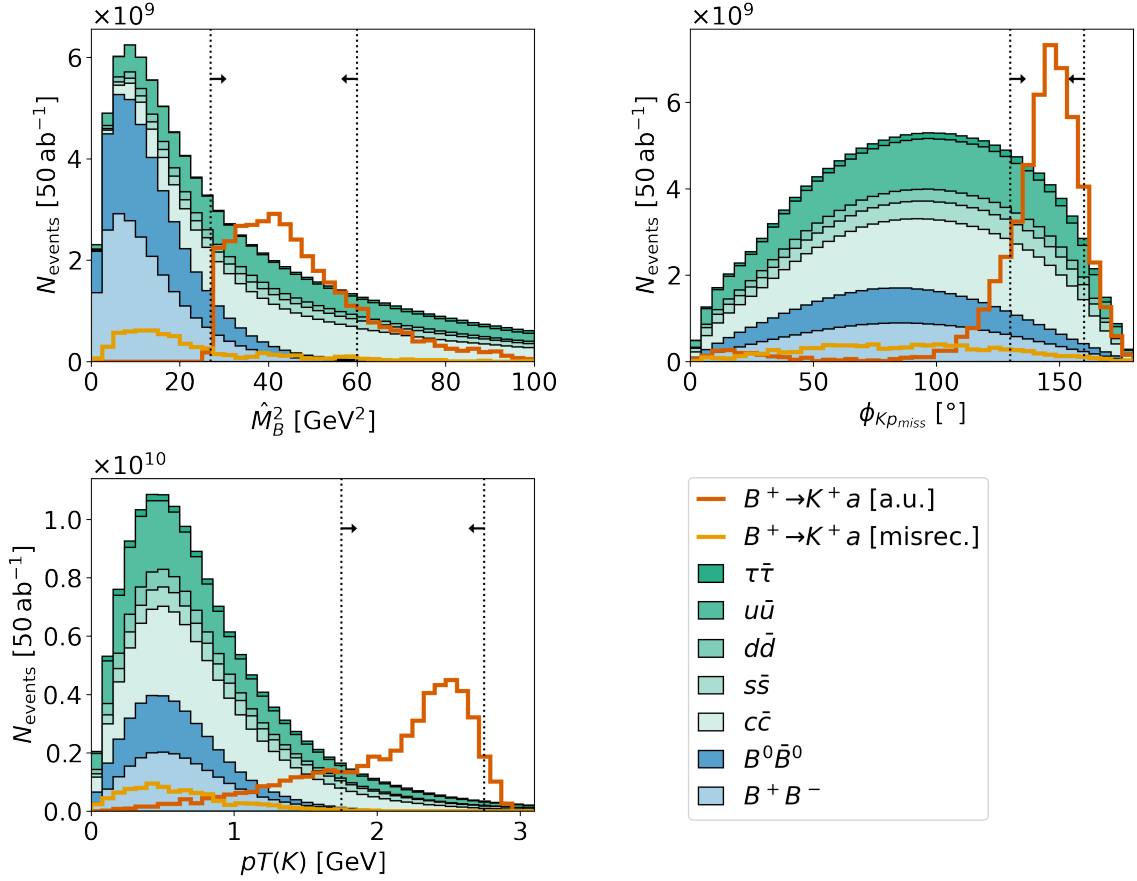
Figure 4: Kinematic distributions of ALPs produced from $B^+ \to K^+ a$ for benchmarks of fixed ALP masses m_a. Top left: reconstructed B meson mass, $\hat{M}_B^2$; top right: opening angle of the leading kaon against the missing momentum, $\phi_{K p_{\mathrm{miss}}}$; bottom left: transverse momentum of the leading kaon, $p_T(K)$. All variables are defined in the lab frame. Shown are signal events (solid curves) and misreconstructed signal events (dotted curves). The number of events is given in arbitrary units. The dotted vertical lines indicate selection cuts; the arrows point toward the signal region.

For background rejection we construct the following three kinematic variables, defined in the lab frame:

- $p_T(K)$ is the transverse momentum of the kaon with the highest transverse momentum in the event, in the following called the *leading kaon*,

- $\hat{M}_B^2 = (E_{\mathrm{miss}} + E_K)^2 - (\vec{p}_{\mathrm{miss}} + \vec{p}_K)^2$ is the reconstructed mass of the signal B meson candidate, i.e., the invariant mass of the leading kaon and missing momenta,

- $\phi_{K p_{\mathrm{miss}}}$ is the angle between the leading kaon and the missing momentum vector, calculated using the four-vectors of all final-state particles and the incoming beams.

Choosing the leading kaon for $p_T(K)$ ensures that only one signal candidate per event exists, but also introduces background from wrongly reconstructed signal candidates with

Figure 5: Kinematic distributions of ALPs produced from $B^+ \to K^+ a$ for a fixed ALP mass $m_a = 300\,\mathrm{MeV}$ and various backgrounds before selections. Top left: reconstructed B meson mass, $\hat{M}_B^2$; top right: opening angle of the leading kaon against the missing momentum, $\phi_{Kp_{\mathrm{miss}}}$; bottom left: transverse momentum of the leading kaon, $p_T(K)$. Signal and misreconstructed signal events are normalised arbitrarily to one tenth of the number of background events. Background events are normalised to the total production rates with $50\,\mathrm{ab}^{-1}$ of data luminosity at Belle II. The dotted vertical lines indicate selection cuts; the arrows point toward the signal region. Figure 7 shows the same distributions after selections.

kaons that belong to the tag-side B meson. We label these events as [*misrec.*] when we illustrate our results.

In Fig. 4 we show the kinematic distributions of the signal events before further kinematic selections for four different ALP mass benchmarks. Kinematic distributions for the various backgrounds and a signal with a fixed mass $m_a = 300\,\mathrm{MeV}$ are shown for comparison in Figs. 5 and 6.

We point out several relevant features: The two-body kinematics of the signal B decay results in a peaking $p_T(K)$ distribution of the leading kaon in the lab frame. The spectrum
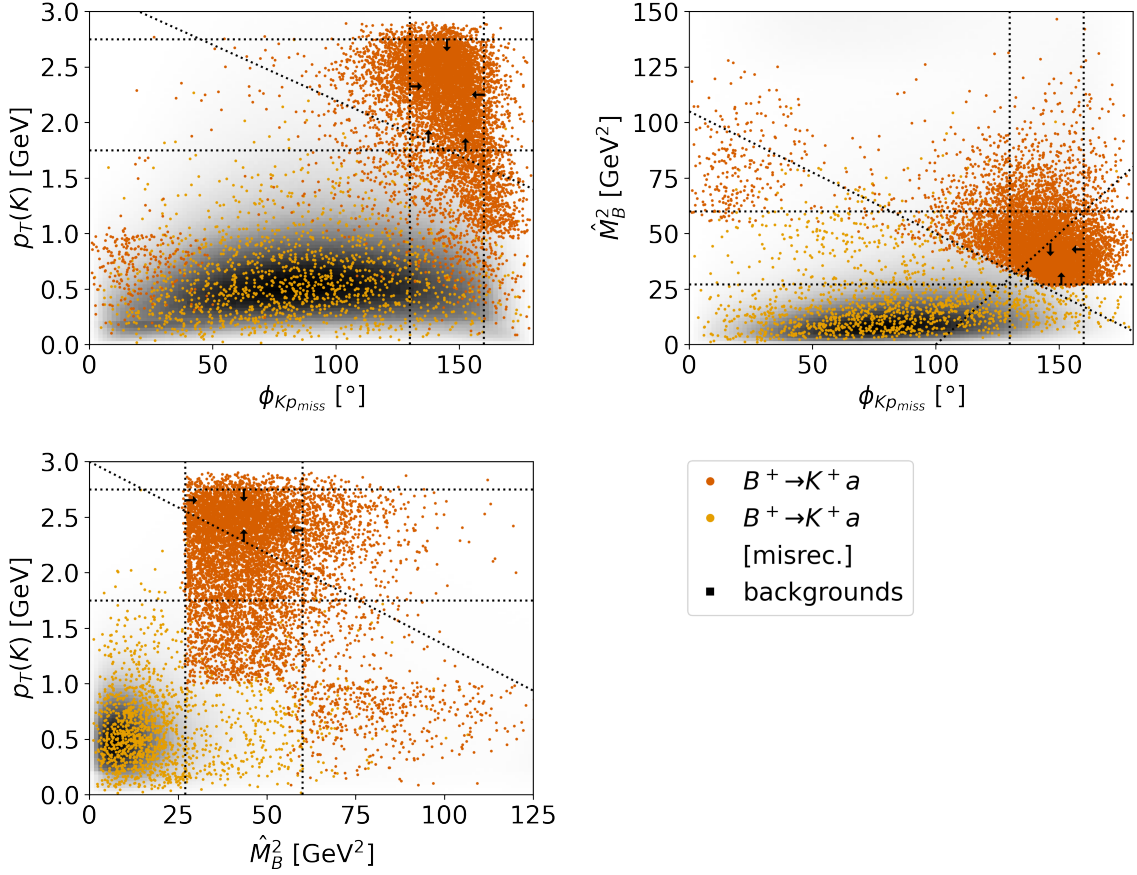
Figure 6: Two-dimensional distributions of the signal (orange points), misreconstructed signal (yellow points), and background (black histograms). Shown are projections of the three-dimensional space of the kinematic variables $p_T(K)$, $\phi_{Kp_{\mathrm{miss}}}$, and $\hat{M}_B^2$. The number of background events corresponds to the full simulated sample of 10 M events per channel. Signal events correspond to a sample of 10 k, which we use here for illustration. The dotted lines indicate selections; the arrows point toward the signal region. Figure 8 shows the same distributions after selections.

for the signal kaon is generally harder than for the background, resulting in a high selection purity.The angular distribution $\phi_{Kp_{\mathrm{miss}}}$ peaks at large angles, as expected from a two-body decay of a slow B meson. The distribution is broadened for heavier ALPs. The reconstruction of $\hat{M}_B^2$ is dominated by the tag-side B meson and hence is largely independent of the ALP mass. The tail of the signal $\hat{M}_B^2$ distribution comes from neutrinos and other missed particles produced from tag-side B decays. For ALP masses below a few hundred MeV all kinematic distributions look identical to the $m_a = 5\,\mathrm{MeV}$ benchmark.

For signal events, the variables $p_T(K)$ and $\phi_{Kp_{\mathrm{miss}}}$ exhibit a rather strong correlation. We also observe a strong, but different correlation of $p_T(K)$ and $\phi_{Kp_{\mathrm{miss}}}$ for misreconstructed signal events, as well as a strong correlation of $\phi_{Kp_{\mathrm{miss}}}$ and $\hat{M}_B^2$. Background events show strong correlations in all combinations of the three variable. We exploit the different corre-

m_a [GeV]	before selection		after selection	
	N_{signal}	$N_{\text{misrec.}}$	N_{signal}	$N_{\text{misrec.}}$
0.005	7802	1442	1091	0
0.3	7823	1453	1022	0
1	7737	1460	770	0
3	7568	1649	0	0

Table 1: Number of signal and misreconstructed signal events before and after applying the selection cuts from (4.1) for various ALP mass benchmarks. The numbers are based on 10k generated signal events. The difference between the number of generated events, N_{gen}, and the sum of signal and misreconstructed events, $N_{\text{signal}} + N_{\text{misrec.}}$, is due to kaons that are out of acceptance or not identified as kaons.

lations for signal and background events and the characteristic shapes of the distributions to optimize our event selection.

To enhance the signal-to-background ratio, we study ALP mass dependent selection criteria using the aforementioned three variables. All selection criteria are chosen to maximize the Punzi figure of merit for a $5\,\sigma$ discovery [70]. For ALP masses $m_a \lesssim 1\,\text{GeV}$, we find that the optimal selections vary little with the ALP mass. We therefore apply one single set of selections to all considered mass benchmarks:

$$1.75 \leq p_T(K) \leq 2.75\,\text{GeV}, \tag{4.1}$$
$$p_T(K) \geq 3.2\,\text{GeV} - 0.01\,\text{GeV}/°\cdot\phi_{Kp_{\text{miss}}},$$
$$p_T(K) \geq 3.0\,\text{GeV} - 0.0165\,\frac{1}{\text{GeV}}\cdot\hat{M}_B^2,$$
$$130° \leq \phi_{Kp_{\text{miss}}} \leq 160°,$$
$$27 \leq \hat{M}_B^2 \leq 60\,\text{GeV}^2,$$
$$\hat{M}_B^2 \geq 105\,\text{GeV}^2 - 0.55\,\text{GeV}^2/°\cdot\phi_{Kp_{\text{miss}}},$$
$$\hat{M}_B^2 \leq -100\,\text{GeV}^2 + 0.992\,\text{GeV}^2/°\cdot\phi_{Kp_{\text{miss}}}.$$

In Figs. 7 and 8 we show the kinematic distributions of the signal for $m_a = 300\,\text{MeV}$ and the remaining backgrounds after applying these selection cuts. We veto events if the ALP decay vertex is within the geometric acceptance of the tracking detectors or the electromagnetic calorimeter, as illustrated in Fig. 9.

After applying the selection cuts from (4.1) and including the detector acceptance, the signal efficiency $\varepsilon = N_{\text{sel}}/N_{\text{gen}}$ ranges around $10\,\%$. Here N_{gen} is the number of generated signal events and N_{sel} is the number of events after selection. In Table 1, we show the number of signal and misreconstructed signal events before and after the selection.

After selection, we have 39 B^+B^- and 28 $B^0\bar{B}^0$ background events left, while no background from $\tau^+\tau^-$ and continuum events remains in generated samples of 10M events per background source. We finally scale these numbers to the event rates corresponding to the
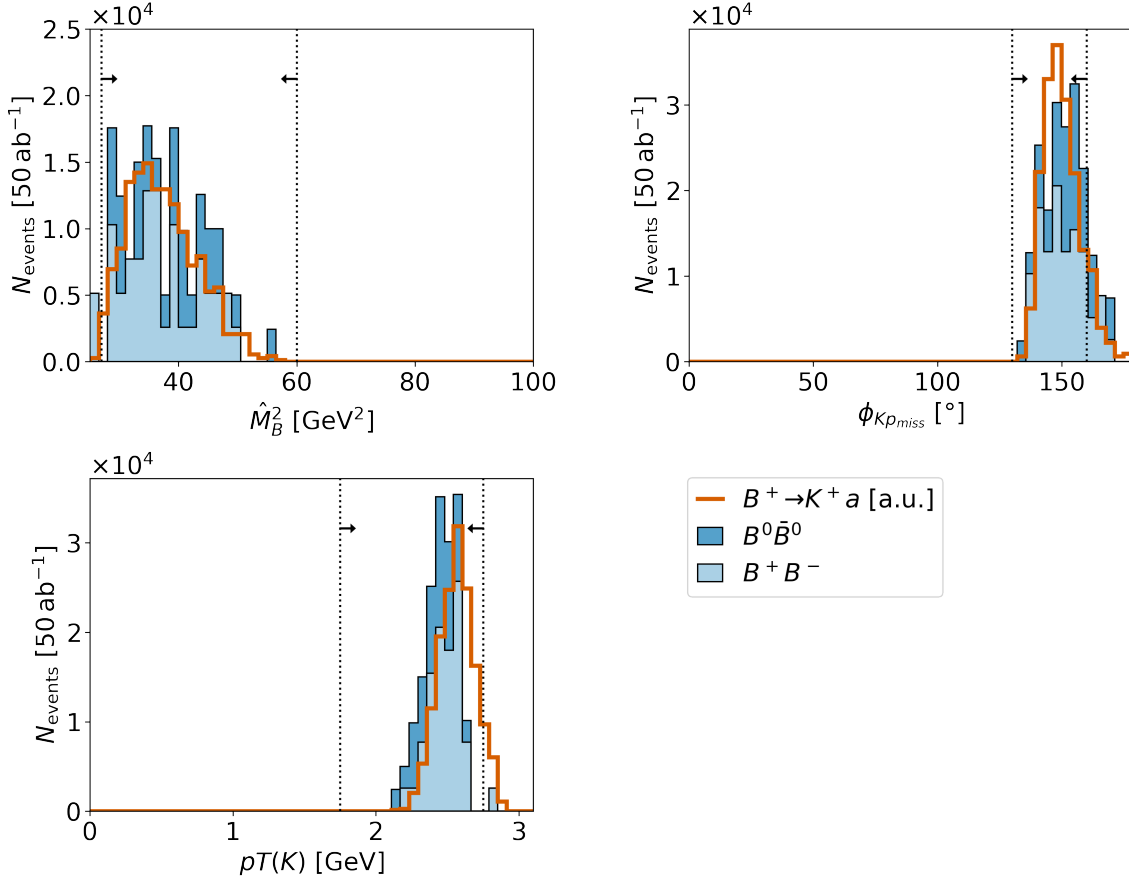
Figure 7: Kinematic distributions of ALPs produced from $B^+ \to K^+ a$ for a fixed ALP mass $m_a = 300\,\mathrm{MeV}$ (orange) and various backgrounds (blue) after selections. Selection cuts have been applied to the respective two variables not shown in the distribution. The dotted lines and arrows denote these selections applied in the direction of the errors. No misreconstructed signal and continuum background events in our respective samples are left after cuts. Signal events are normalised arbitrarily to five times the number of background events. Background events are normalised to the total production rates with $50\,\mathrm{ab}^{-1}$ of data luminosity at Belle II. Figure 5 shows the same distributions after selections.

respective integrated luminosity. This procedure potentially underestimates background from $\tau^+\tau^-$ and continuum events due to our limited background statistics. Based on our studies we assume that the dominant background comes from B^+B^- and $B^0\bar{B}^0$ events.

4.3 Projected sensitivity

For each ALP mass scenario, we derive an expected 90% CL upper limit on the observed number of signal events, N_S, based on the expected number of background events, N_B. Here N_B is the number of simulated background events after our selection procedure, scaled to the respective integrated luminosity. In each ALP mass scenario, the 90% CL upper limit on the signal rate, N_S, is determined iteratively, such that the Poisson probability of
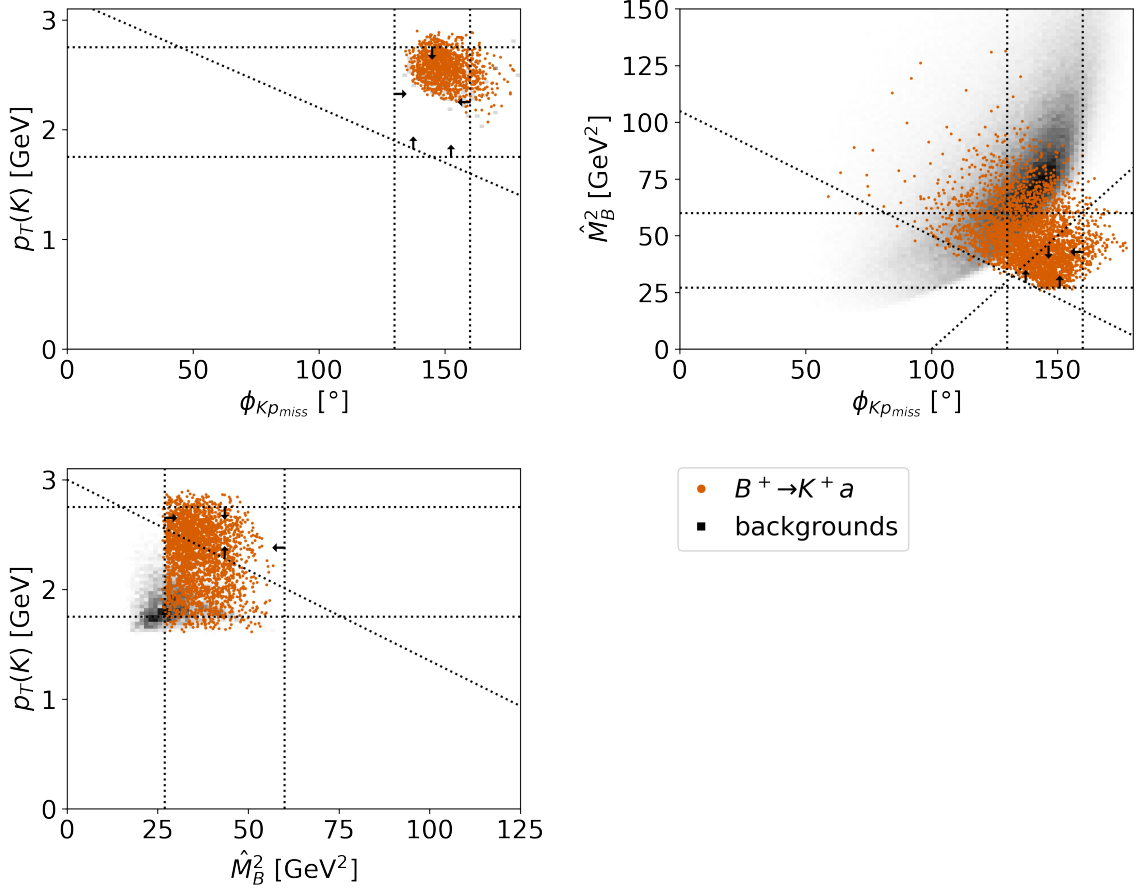
Figure 8: Two-dimensional phase-space distributions of the signal (orange points) and background (black histograms) after selections. Shown are projections of the three-dimensional space of the kinematic variables $p_T(K)$, $\phi_{Kp_{\rm miss}}$, and $\hat{M}_B^2$. Selection cuts have been applied to the respective third variable not shown in the panel. The dotted lines indicate the selection cuts; the arrows point toward the signal region. No misreconstructed signal events are left after selections. The number of background events corresponds to the full simulated sample of $10\,\mathrm{M}$ events per channel. Signal events correspond to a sample of $10\,\mathrm{k}$ for illustration. Figure 6 shows the corresponding distributions before selections.

observing N events when predicting $N_S + N_B$ events is 0.1. Here N is the integer closest to the number of expected background events N_B. In this way, we derive upper bounds on the branching ratio $\mathcal{B}(B^+ \to K^+ a)$ by requiring

$$N_S \geq N_{B\bar{B}} \cdot \mathcal{B}(B^+ \to K^+ a) \cdot \langle \mathbb{P}_a \rangle. \tag{4.2}$$

The projected upper limits on $\mathcal{B}(B^+ \to K^+ a)$ are shown as a function of the ALP decay length $c\tau_a$ in Fig. 10. We interpret these bounds in terms of the couplings c_{ff} and c_{WW}; the results are shown in Fig. 11. To obtain the bound as a function of the ALP mass and couplings, we use the root-finding algorithm `scipy.optimize.fsolve` [71] and show an additional, optimistic, projected limit for the case that the background is reduced to zero.
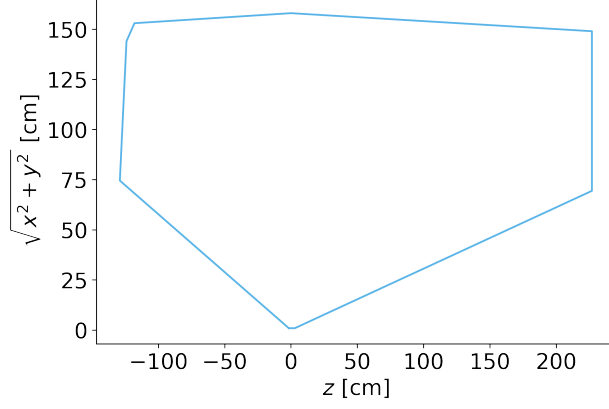
Figure 9: Schematic drawing of the Belle II detector used to select invisible ALP decays. The displayed geometry includes the central drift chamber and the calorimeter, as specified in the text. The detector is assumed to be symmetric around the beam axis z.
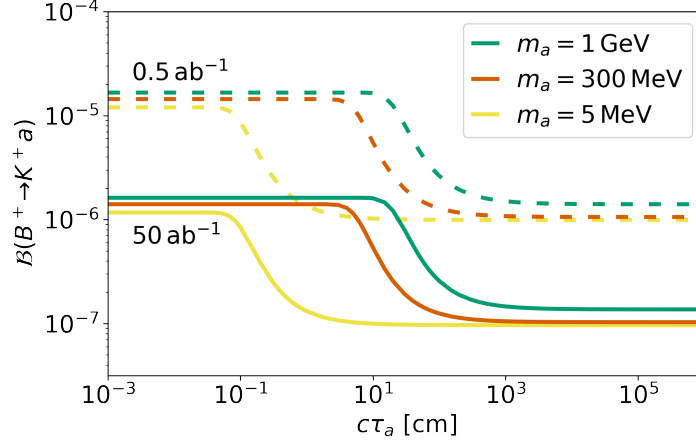
Figure 10: Projected 90 % CL upper limits on the branching ratio $\mathcal{B}(B^+ \to K^+ a)$ of an invisibly decaying ALP or similar (pseudo-)scalar resonance a from $B^+ \to K^+ a$, $a \to \not{E}$ at Belle II. The projected limits are shown for fixed ALP masses as a function of the ALP decay length $c\tau_a$, for 0.5 ab^{-1} (dashed) and 50 ab^{-1} (solid) of data.

All curves feature a mass-dependent kink. For ALP masses below this kink, the ALP can be considered stable at the scale of the Belle II vertex detector. For ALP masses above the kink, the decay length of the ALP is shorter than the detector radius, but the ALP can still appear invisible due to the limited acceptance and reconstruction efficiency. In this way, searches for $B^+ \to K^+ \not{E}$ are sensitive to even short-lived light resonances, which a priori could be expected to decay within the detector.

We finally show our projected sensitivity for $B^+ \to K^+ \not{E}$ together with existing bounds from other searches in Fig. 12.
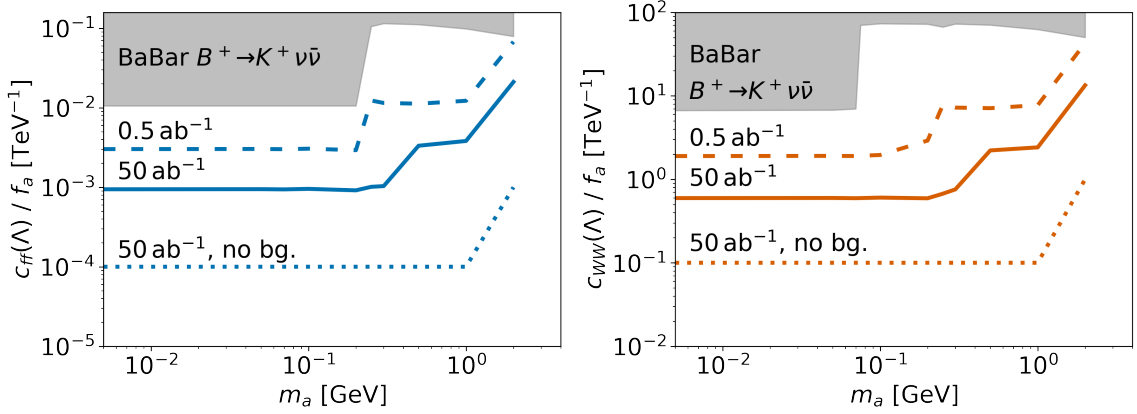
Figure 11: Projected $90\,\%$-CL upper limits on the couplings c_{ff} (left) and c_{WW} (right) in our two scenarios. The solid lines denote the full Belle II luminosity of $50\,\text{ab}^{-1}$ and dashed lines denote the current integrated luminosity $0.5\,\text{ab}^{-1}$, both with the full background considered. The dotted line shows the limit with full $50\,\text{ab}^{-1}$ luminosity for the case that the background is reduced to zero. The shaded regions show the BaBar bound from $B^+ \to K^+\nu\bar{\nu}$ for comparison.

5 Displaced ALP decays at Belle II

As discussed in Sec. 3, current bounds show a complementarity of invisible and displaced searches when scanning the ALP parameter space, see Fig. 3. Indeed, for a fixed coupling, light ALPs are produced with a large boost and tend to decay outside of a detector, leaving signatures with missing momentum. Heavier ALPs, on the other hand, are more likely to decay within the detector volume and can be detected through displaced decay products.

To complement our analysis of invisible ALPs at Belle II from Sec. 4, we assess the reach of displaced signatures at Belle II. We build our analysis on a recent study of dark scalars S in $B^+ \to K^+S$, $S \to X$ [20] for leptonic final states $X = \{e^+e^-, \mu^+\mu^-\}$. Since both the dark scalar and the ALP are bosons with spin zero, their kinematic distributions in the relevant decay chains are the same. This allows us to rerun the analysis for ALPs, using the production rate, lifetime and decay branching ratios from Sec. 2. Following the procedure of Sec. IV in Ref. [20], we calculate the number of displaced lepton pairs from ALP decays within the Belle II tracking detector for the two ALP scenarios.

In Fig. 12, we show contours of 2.3 expected signal events from $B^+ \to K^+a$, $a \to \{e^+e^-, \mu^+\mu^-\}$ decays at Belle II in $50\,\text{ab}^{-1}$ of data. The regions inside the contours would be excluded at the 90% CL by a non-observation of ALP decays, assuming zero background. For a given ALP mass, the sensitivity to larger couplings is limited by the minimum radial displacement required for the ALP decay products to be $d > 0.9\,\text{cm}$. The sensitivity to small couplings is limited by the ALP production rate. In the c_{ff} scenario, the sudden changes in sensitivity at $m_a \approx 0.2\,\text{GeV}$ and $1\,\text{GeV}$ are due to changes in the ALP branching ratios, see Fig. 1. The sensitivity cutoff at $m_a \sim 1\,\text{GeV}$ for electrons and $m_a \sim 2.5\,\text{GeV}$ for
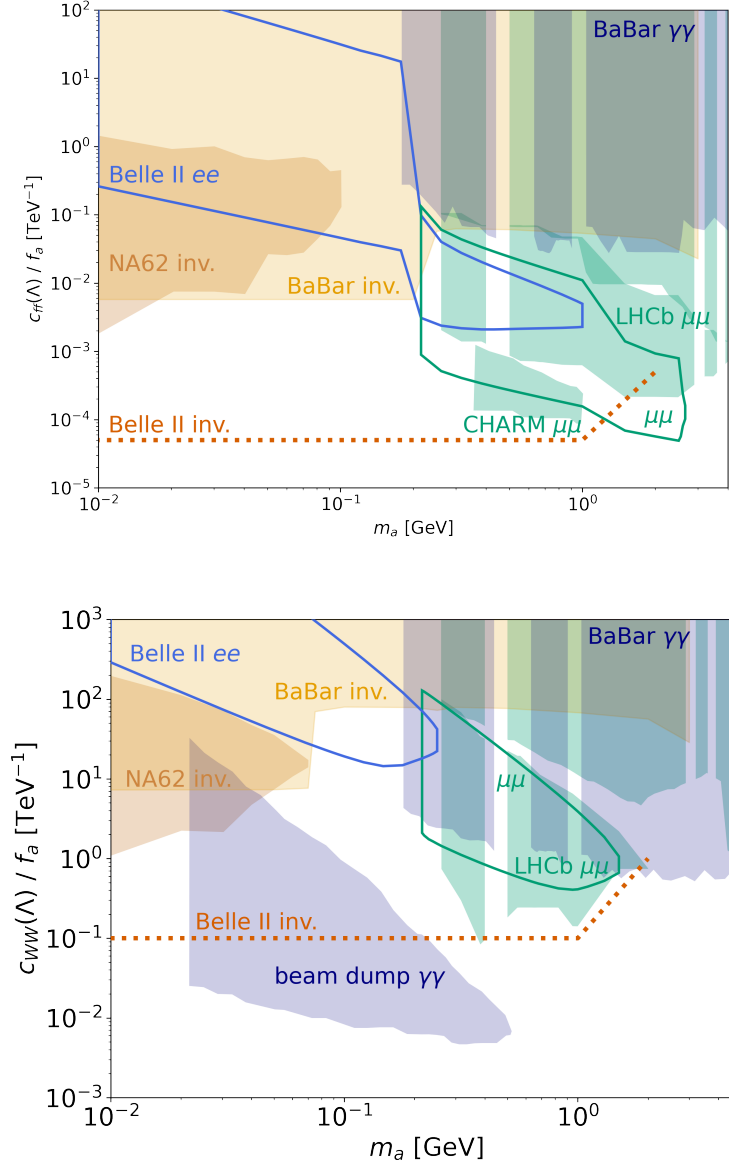
Figure 12: Projections for Belle II's sensitivity to ALPs with effective couplings to fermions, $c_{ff}(\Lambda)/f_a$ (top), and weak gauge bosons, $c_{WW}(\Lambda)/f_a$ (bottom), as a function of the ALP mass m_a. Shown are contours of $N = 2.3$ events expected in $50\,\mathrm{ab}^{-1}$ of data from $B^+ \to K^+ a$, $a \to X$ decays with $X = e^+e^-$ (blue) and $\mu^+\mu^-$ (green). The area enclosed by the contours could be excluded at the 90% CL, assuming zero background. The region above the orange dashed curve (cf. Fig. 11) could be excluded at 90% CL with the search for $B^+ \to K^+ a$, $a \to$ inv. proposed in Sec. 4, assuming zero background. For comparison, we also show the existing bounds on ALPs from Fig. 3.

muons are also largely due to drops in the ALP branching ratios. In the c_{ff} scenario the sensitivity to displaced leptons is expected to dominate due to the large branching ratio into leptons; for the c_{WW} scenario the sensitivity to photons is more promising. Searches

for $B^+ \to K^+a, a \to \gamma\gamma$ at Belle II can be interesting probes of long-lived ALPs with dominant electroweak couplings. A recent such search by BaBar [44], shown in blue in Fig. 12, suggests that Belle II has good potential to explore photon final states. For a realistic prediction of the reach, however, the reconstruction efficiency for photon pairs and the background in displaced di-photon searches have to be assessed.

To compare the reach of displaced and invisible signatures at Belle II, we also show the projections for $B^+ \to K^+a$, $a \to$ inv. from Fig. 11 for zero background (orange dotted curves). For a fixed coupling, displaced searches are most sensitive at high ALP masses, while invisible searches appear to be much more sensitive to lighter ALPs with $m_a < 1\,\text{GeV}$. For a more accurate comparison of the two searches, a detailed study of backgrounds for the displaced ALP signatures would be required.

In combination, displaced and invisible signatures at Belle II can set mass-dependent upper bounds on the ALP couplings

$$c_{ff}(\Lambda)/f_a \lesssim (5 \cdot 10^{-5} - 10^{-4})\,\text{TeV}^{-1}, \qquad c_{WW}(\Lambda)/f_a \lesssim 10^{-1}\,\text{TeV}^{-1}, \qquad (5.1)$$

improving the current reach by up to two orders of magnitude, see (3.8), and covering unexplored parameter space at larger couplings. Due to the high projected sensitivity to $B^+ \to K^+a$, $a \to$ inv. even at moderate ALP lifetimes, signatures with missing energy play an important role in probing such feeble interactions. In the case of an observed excess in $B \to K\!\!\!/E$ decays, searches for displaced visible ALP decays will provide a valuable independent test of the underlying model.

6   Conclusions

The purpose of this paper was to assess Belle II's sensitivity to displaced versus invisibly decaying light resonances produced from meson decays. To this end, we have developed a new search strategy for invisibly decaying ALPs in meson decays $B^+ \to K^+a$, $a \to \!\!\!/E$.

The search for $B^+ \to K^+\!\!\!/E$ is optimized for two-body decays and is inclusive in the decay modes of the second B meson from $B\bar{B}$ pairs produced at Belle II. We have performed a detailed analysis of the signal and background kinematics and identified three variables as very sensitive to $B^+ \to K^+\!\!\!/E$: the reconstructed B meson mass squared, $\hat{M}_B^2$; the transverse momentum of the kaon, $p_T(K)$; and the angle between the kaon and the missing momentum, $\phi_{Kp_{\text{miss}}}$, the latter being reconstructed indirectly from the visible decay products. With suitable selections based on three kinematic variables, we were able to determine a signal region that is largely free from SM background and misreconstructed $B^+ \to K^+a$ decays.

For ALPs with decay lengths $c\tau_a \gtrsim 1\,\text{cm}$, we find that Belle II can probe rates of $\mathcal{B}(B^+ \to K^+a) \gtrsim 10^{-7}$ with $50\,\text{ab}^{-1}$ of data. Remarkably, the search is also sensitive to short-lived ALPs, which might escape the detector due to the limited angular coverage. For ALPs with decay lengths $c\tau_a \lesssim 1\,\text{cm}$, we expect Belle II to be sensitive to $\mathcal{B}(B^+ \to K^+a) \gtrsim 10^{-6}$ with $50\,\text{ab}^{-1}$. The sensitivity can be further enhanced with a multi-variate analysis. With the

$0.5\,\mathrm{ab}^{-1}$ of data expected in 2022, Belle II can already probe ALPs with smaller production rates than our reinterpretation of a search for $B^+ \to K^+ \nu\bar{\nu}$ by BaBar.

To compare our predictions for $B^+ \to K^+ \not{E}$ with searches for displaced particles at Belle II, we have estimated the reach of $B^+ \to K^+ a$, $a \to X$ with $X = \{e^+e^-, \mu^+\mu^-\}$ for two specific scenarios with ALPs coupling to fermions and weak gauge bosons, respectively. For ALPs with masses below about $1\,\mathrm{GeV}$, $B^+ \to K^+ \not{E}$ can probe couplings up to several orders of magnitude smaller than $B^+ \to K^+ X$. For heavier ALPs, we expect that searches for displaced particles can be more sensitive.

Compared with existing collider searches for displaced and invisible light resonances, Belle II can significantly improve the sensitivity to small ALP couplings, see Fig. 12. For sub-GeV ALPs, the sensitivity of $B^+ \to K^+ \not{E}$ even exceeds the reach of long-baseline experiments like NA62 and CHARM and is competitive with high-intensity beam-dump experiments like NuCal and E137.

For ALPs with predominant couplings to photons, we expect a significantly improved sensitivity also from approved experiments like FASER, NA62-dump, and NA64e in the near future [2]. An even better sensitivity may be reached by the proposed experiments SHiP, FASER2, or ultimately at a Gamma Factory in the far future. For ALPs with predominant couplings to fermions, the proposed beam-dump experiment SHADOWS [72] might reach the best sensitivity, while ultimate sensitivity can be reached by the proposed experiments KLEVER (low mass) and MATHUSLA (high mass) [2].

Our predictions for $B^+ \to K^+ \not{E}$ and $B^+ \to K^+ X$ at Belle II apply in a very similar way to other light pseudo-scalar or scalar resonances. Belle II has just started to exploit its discovery potential for light new particles with signatures of displaced vertices or missing energy. We hope that this analysis will be used as a guideline for future searches.

Acknowledgments

A   ALP decay widths

For convenience, we summarize the partial decay widths of the ALP in terms of its mass m_a and couplings c_{ii}. All couplings are defined at the ALP mass scale, $c_{ii} = c_{ii}(m_a)$. In large parts, the formulas below correspond with the results of Ref. [36].

The ALP decay widths into fermions is given by

$$\Gamma_{a \to f\bar{f}} = 2\pi m_a N_c^f \frac{|c_{ff}(m_a)|^2 m_f^2}{\Lambda^2} \left(1 - \frac{4m_f^2}{m_a^2}\right)^{\frac{1}{2}} + \mathcal{O}\left(\frac{\alpha^2}{(4\pi)^2} c_{WW}\right), \quad f = \{q, \ell\} \quad \text{(A.1)}$$

where $N_c^\ell = 1$, $N_c^q = 3$. The decay width into hadrons reads

$$\Gamma_{a \to \text{had}} = \frac{2\alpha_s^2 m_a^3}{\pi} \frac{|C_{GG}^{\text{eff}}(m_a)|^2}{\Lambda^2} \left(1 + \left(\frac{97}{4} - \frac{7n_q}{6}\right)\frac{\alpha_s}{\pi}\right) + \sum_q \Gamma_{a \to q\bar{q}}, \quad \text{(A.2)}$$

where $n_q = 3$ is the number of light quarks $q = \{u, d, s\}$ and the effective gluon coupling is given by

$$C_{GG}^{\text{eff}}(m_a) = c_{GG}(m_a) + \sum_{q'} \frac{c_{q'q'}(m_a)}{2} B_1\left(\frac{4m_{q'}^2}{m_a^2}\right) \quad \text{(A.3)}$$

where q' are all quarks with $m_{q'} \lesssim m_a$. We use $\Gamma_{a \to \text{had}}$ for ALP masses above $1\,\text{GeV}$. For $m_a < 1\,\text{GeV}$, we approximate the hadronic decay width of the ALP by the decay width into three pions,

$$\Gamma_{a \to \pi^0 \pi^i \pi^j} = \frac{m_a m_\pi^4}{384\pi f_\pi^2 \Lambda^2} \left(c_{uu}(m_a) - c_{dd}(m_a) + 2c_{GG}(m_a)\frac{m_d - m_u}{m_d + m_u}\right)^2 g_{ij}\left(\frac{m_\pi^2}{m_a^2}\right), \quad \text{(A.4)}$$

with

$$g_{00}(r) = \frac{2}{(1-r)^2} \int_{4r}^{(1-\sqrt{r})^2} \mathrm{d}z \sqrt{1 - 4\frac{r}{z}} \sqrt{\lambda(1, z, r)} \quad \text{(A.5)}$$

$$g_{+-}(r) = \frac{12}{(1-r)^2} \int_{4r}^{(1-\sqrt{r})^2} \mathrm{d}z \sqrt{1 - 4\frac{r}{z}} \sqrt{\lambda(1, z, r)}\, (z - r)^2$$

and $\lambda(a, b, c) = a^2 + b^2 + c^2 - 2ab - 2bc - 2ca$.

The decay width of the ALP into photons is given by

$$\Gamma_{a \to \gamma\gamma} = \frac{\alpha^2 m_a^3}{4\pi\Lambda^2} \left|C_{\gamma\gamma}^{\text{eff}}(m_a)\right|^2, \quad \text{(A.6)}$$

with

$$C_{\gamma\gamma}^{\text{eff}}(m_a) = \begin{cases} c_{\gamma\gamma}(m_a) + \sum\limits_{f \in \{\ell, Q\}} N_c^f Q_f^2 c_{ff}(m_a) B_1\left(\frac{4m_f^2}{m_a^2}\right) & m_a > 1\,\text{GeV} \\[2ex] c_{\gamma\gamma}(m_a) + \sum\limits_{f \in \{\ell, Q\}} N_c^f Q_f^2 c_{ff}(m_a) B_1\left(\frac{4m_f^2}{m_a^2}\right) & \\[2ex] \quad - \frac{m_a^2}{m_\pi^2 - m_a^2} \frac{c_{uu}(m_a) - c_{dd}(m_a)}{2} - \left(\frac{5}{3} + \frac{m_\pi^2}{m_\pi^2 - m_a^2}\frac{m_d - m_u}{m_d + m_u}\right) c_{GG}(m_a) & m_a < 1\,\text{GeV}, \end{cases} \quad \text{(A.7)}$$

where $\ell \in \{e, \mu, \tau\}$, $Q \in \{c, b, t\}$ and

$$B_1(\tau) = 1 - \tau f^2(\tau) \tag{A.8}$$

$$f(\tau) = \begin{cases} \arcsin \frac{1}{\sqrt{\tau}} & \tau \geq 1 \\ \frac{\pi}{2} + \frac{i}{2} \ln \frac{1+\sqrt{1-\tau}}{1-\sqrt{1-\tau}} & \tau < 1 \end{cases}.$$

References

[1] G. Lanfranchi, M. Pospelov, and P. Schuster, *The Search for Feebly-Interacting Particles,* 2011.02157.

[2] P. Agrawal et al., *Feebly-interacting particles: FIPs 2020 workshop report,* Eur. Phys. J. C **81** (2021), no. 11 1015, [2102.12143].

[3] M. Borsato et al., *Unleashing the full power of LHCb to probe Stealth New Physics,* 2105.12668.

[4] **FASER**, A. Ariga et al., *FASER: ForwArd Search ExpeRiment at the LHC,* 1901.04468.

[5] B. Döbrich, J. Jaeckel, and T. Spadaro, *Light in the beam dump - ALP production from decay photons in proton beam-dumps,* JHEP **05** (2019) 213, [1904.02091]. [Erratum: JHEP 10, 046 (2020)].

[6] Y.-D. Tsai, P. deNiverville, and M. X. Liu, *Dark Photon and Muon $g - 2$ Inspired Inelastic Dark Matter Models at the High-Energy Intensity Frontier,* Phys. Rev. Lett. **126** (2021), no. 18 181801, [1908.07525].

[7] **NA64**, D. Banerjee et al., *Search for Axionlike and Scalar Particles with the NA64 Experiment,* Phys. Rev. Lett. **125** (2020), no. 8 081801, [2005.02710].

[8] **NA62**, E. Cortina Gil et al., *Search for a feebly interacting particle X in the decay $K^+ \to \pi^+ X$,* JHEP **03** (2021) 058, [2011.11329].

[9] **NA62**, E. Cortina Gil et al., *Measurement of the very rare $K^+ \to \pi^+ \nu \bar\nu$ decay,* JHEP **06** (2021) 093, [2103.15389].

[10] J. Alimena et al., *Searching for long-lived particles beyond the Standard Model at the Large Hadron Collider,* J. Phys. G **47** (2020), no. 9 090501, [1903.04497].

[11] M. Duerr, T. Ferber, C. Hearty, F. Kahlhoefer, K. Schmidt-Hoberg, et al., *Invisible and displaced dark matter signatures at Belle II,* JHEP **02** (2020) 039, [1911.03176].

[12] M. Duerr, T. Ferber, C. Garcia-Cely, C. Hearty, and K. Schmidt-Hoberg, *Long-lived Dark Higgs and Inelastic Dark Matter at Belle II,* JHEP **04** (2021) 146, [2012.08595].

[13] M. Beltran, D. Hooper, E. W. Kolb, Z. A. C. Krusberg, and T. M. P. Tait, *Maverick dark matter at colliders,* JHEP **09** (2010) 037, [1002.4137].

[14] J. Goodman, M. Ibe, A. Rajaraman, W. Shepherd, T. M. P. Tait, et al., *Constraints on Dark Matter from Colliders,* Phys. Rev. D **82** (2010) 116010, [1008.1783].

[15] **LHC Dark Matter Working Group**, T. Abe et al., *LHC Dark Matter Working Group: Next-generation spin-0 dark matter models,* Phys. Dark Univ. **27** (2020) 100351, [1810.09420].

[16] **Belle II**, F. Abudinén et al., *Search for $B^+ \to K^+ \nu \bar\nu$ decays using an inclusive tagging method at Belle II,* 2104.12624.

[17] **BaBar**, J. P. Lees et al., *Search for Long-Lived Particles in e^+e^- Collisions*, Phys. Rev. Lett. **114** (2015), no. 17 171801, [`1502.02580`].

[18] **BaBar**, J. P. Lees et al., *Search for a Dark Leptophilic Scalar in e^+e^- Collisions*, Phys. Rev. Lett. **125** (2020), no. 18 181801, [`2005.01885`].

[19] **Belle**, D. Liventsev et al., *Search for heavy neutrinos at Belle*, Phys. Rev. D **87** (2013), no. 7 071102, [`1301.1105`]. [Erratum: Phys.Rev.D 95, 099903 (2017)].

[20] A. Filimonova, R. Schäfer, and S. Westhoff, *Probing dark sectors with long-lived particles at BELLE II*, Phys. Rev. D **101** (2020), no. 9 095006, [`1911.03490`].

[21] E. Bertholet, S. Chakraborty, V. Loladze, T. Okui, A. Soffer, et al., *Heavy QCD Axion at Belle II: Displaced and Prompt Signals*, `2108.10331`.

[22] **BaBar**, J. P. Lees et al., *Search for $B \to K^{(*)}\nu\overline{\nu}$ and invisible quarkonium decays*, Phys. Rev. D **87** (2013), no. 11 112005, [`1303.7465`].

[23] **Belle**, J. Grygier et al., *Search for $B \to h\nu\bar{\nu}$ decays with semileptonic tagging at Belle*, Phys. Rev. D **96** (2017), no. 9 091101, [`1702.03224`]. [Addendum: Phys.Rev.D 97, 099902 (2018)].

[24] R. D. Peccei and H. R. Quinn, *CP Conservation in the Presence of Instantons*, Phys. Rev. Lett. **38** (1977) 1440–1443.

[25] R. D. Peccei and H. R. Quinn, *Constraints Imposed by CP Conservation in the Presence of Instantons*, Phys. Rev. D **16** (1977) 1791–1797.

[26] S. Weinberg, *A New Light Boson?*, Phys. Rev. Lett. **40** (1978) 223–226.

[27] F. Wilczek, *Problem of Strong P and T Invariance in the Presence of Instantons*, Phys. Rev. Lett. **40** (1978) 279–282.

[28] C. Bobeth, T. Ewerth, F. Kruger, and J. Urban, *Analysis of neutral Higgs boson contributions to the decays $\bar{B}_s \to \ell^+\ell^-$ and $\bar{B} \to K\ell^+\ell^-$*, Phys. Rev. D **64** (2001) 074014, [`hep-ph/0104284`].

[29] G. Hiller, *B physics signals of the lightest CP odd Higgs in the NMSSM at large tan beta*, Phys. Rev. D **70** (2004) 034018, [`hep-ph/0404220`].

[30] S. Andreas, O. Lebedev, S. Ramos-Sanchez, and A. Ringwald, *Constraints on a very light CP-odd Higgs of the NMSSM and other axion-like particles*, JHEP **08** (2010) 003, [`1005.3978`].

[31] M. Freytsis, Z. Ligeti, and J. Thaler, *Constraining the Axion Portal with $B \to Kl^+l^-$*, Phys. Rev. D **81** (2010) 034001, [`0911.5355`].

[32] B. Batell, M. Pospelov, and A. Ritz, *Multi-lepton Signatures of a Hidden Sector in Rare B Decays*, Phys. Rev. D **83** (2011) 054005, [`0911.4938`].

[33] M. J. Dolan, F. Kahlhoefer, C. McCabe, and K. Schmidt-Hoberg, *A taste of dark matter: Flavour constraints on pseudoscalar mediators*, JHEP **03** (2015) 171, [`1412.5174`]. [Erratum: JHEP 07, 103 (2015)].

[34] E. Izaguirre, T. Lin, and B. Shuve, *Searching for Axionlike Particles in Flavor-Changing Neutral Current Processes*, Phys. Rev. Lett. **118** (2017), no. 11 111802, [`1611.09355`].

[35] H. Georgi, D. B. Kaplan, and L. Randall, *Manifesting the Invisible Axion at Low-energies*, Phys. Lett. B **169** (1986) 73–78.

[36] M. Bauer, M. Neubert, S. Renner, M. Schnubel, and A. Thamm, *The Low-Energy Effective Theory of Axions and ALPs,* JHEP **04** (2021) 063, [2012.12272].

[37] K. Choi, S. H. Im, C. B. Park, and S. Yun, *Minimal Flavor Violation with Axion-like Particles,* JHEP **11** (2017) 070, [1708.00021].

[38] J. Martin Camalich, M. Pospelov, P. N. H. Vuong, R. Ziegler, and J. Zupan, *Quark Flavor Phenomenology of the QCD Axion,* Phys. Rev. D **102** (2020), no. 1 015023, [2002.04623].

[39] M. Chala, G. Guedes, M. Ramos, and J. Santiago, *Running in the ALPs,* Eur. Phys. J. C **81** (2021), no. 2 181, [2012.09017].

[40] We thank Sebastian Bruggisser and Lara Grabitz for sharing their code with us.

[41] N. Gubernari, A. Kokulu, and D. van Dyk, *B → P and B → V Form Factors from B-Meson Light-Cone Sum Rules beyond Leading Twist,* JHEP **01** (2019) 150, [1811.00983].

[42] M. Bauer, M. Neubert, and A. Thamm, *Collider Probes of Axion-Like Particles,* JHEP **12** (2017) 044, [1708.00443].

[43] **LHCb**, R. Aaij et al., *Search for long-lived scalar particles in $B^+ \to K^+\chi(\mu^+\mu^-)$ decays,* Phys. Rev. D **95** (2017), no. 7 071101, [1612.07818].

[44] **BaBar**, *Search for an Axion-Like Particle in B Meson Decays,* 2111.01800.

[45] **NA48/2**, J. R. Batley et al., *New measurement of the $K^\pm \to \pi^\pm\mu+\mu-$ decay,* Phys. Lett. B **697** (2011) 107–115, [1011.4817].

[46] **LHCb**, R. Aaij et al., *Search for hidden-sector bosons in $B^0 \to K^{*0}\mu^+\mu^-$ decays,* Phys. Rev. Lett. **115** (2015), no. 16 161802, [1508.04094].

[47] B. Döbrich, F. Ertas, F. Kahlhoefer, and T. Spadaro, *Model-independent bounds on light pseudoscalars from rare B-meson decays,* Phys. Lett. B **790** (2019) 537–544, [1810.11336].

[48] **LHCb**, R. Aaij et al., *Searches for low-mass dimuon resonances,* JHEP **10** (2020) 156, [2007.03923].

[49] F. Bergsma, J. Dorenbosch, J. Allaby, U. Amaldi, G. Barbiellini, et al., *Search for axion-like particle production in 400 gev proton-copper interactions,* Physics Letters B **157** (1985), no. 5 458–462.

[50] M. W. Winkler, *Decay and detection of a light scalar boson mixing with the Higgs boson,* Phys. Rev. D **99** (2019), no. 1 015018, [1809.01876].

[51] **NA48/2**, J. R. Batley et al., *Precise measurement of the $K^\pm \to \pi^\pm e+e-$ decay,* Phys. Lett. B **677** (2009) 246–254, [0903.3130].

[52] M. J. Dolan, T. Ferber, C. Hearty, F. Kahlhoefer, and K. Schmidt-Hoberg, *Revised constraints and Belle II sensitivity for visible and invisible axion-like particles,* JHEP **12** (2017) 094, [1709.00009]. [Erratum: JHEP 03, 190 (2021)].

[53] **E949**, A. V. Artamonov et al., *Search for the decay $K^+ \to \pi^+\gamma\gamma$ in the π^+ momentum region $P > 213$ MeV/c,* Phys. Lett. B **623** (2005) 192–199, [hep-ex/0505069].

[54] **Belle II**, F. Abudinén et al., *Search for Axion-Like Particles produced in e^+e^- collisions at Belle II,* Phys. Rev. Lett. **125** (2020), no. 16 161806, [2007.13071].

[55] S. Knapen, T. Lin, H. K. Lou, and T. Melia, *Searching for Axionlike Particles with Ultraperipheral Heavy-Ion Collisions,* Phys. Rev. Lett. **118** (2017), no. 17 171801, [1607.06083].

[56] N. Carrasco, P. Lami, V. Lubicz, L. Riggio, S. Simula, et al., *K → π semileptonic form factors with $N_f = 2 + 1 + 1$ twisted mass fermions,* Phys. Rev. D **93** (2016), no. 11 114512, [1602.04113].

[57] C.-Y. Seng, D. Galviz, W. J. Marciano, and U.-G. Meißner, *An update on $|V_{us}|$ and $|V_{us}/V_{ud}|$ from semileptonic kaon and pion decays,* 2107.14708.

[58] **NA62**, E. Cortina Gil et al., *Search for π^0 decays to invisible particles,* JHEP **02** (2021) 201, [2010.07644].

[59] **KOTO**, J. K. Ahn et al., *Search for the $K_L → \pi^0 \nu \bar{\nu}$ and $K_L → \pi^0 X^0$ decays at the J-PARC KOTO experiment,* Phys. Rev. Lett. **122** (2019), no. 2 021802, [1810.09655].

[60] **Belle II Framework Software Group**, T. Kuhr, C. Pulvermacher, M. Ritter, T. Hauth, and N. Braun, *The Belle II Core Software,* Comput. Softw. Big Sci. **3** (2019), no. 1 1, [1809.04299].

[61] **Belle II**, *Belle II Analysis Software Framework (basf2): release-06-00-00,* Oct., 2021.

[62] D. J. Lange, *The EvtGen particle decay simulation package,* Nucl. Instrum. Meth. A **462** (2001) 152–155.

[63] S. Jadach, B. F. L. Ward, and Z. Was, *The Precision Monte Carlo event generator KK for two fermion final states in e+ e- collisions,* Comput. Phys. Commun. **130** (2000) 260–325, [hep-ph/9912214].

[64] T. Sjöstrand, S. Ask, J. R. Christiansen, R. Corke, N. Desai, et al., *An introduction to PYTHIA 8.2,* Comput. Phys. Commun. **191** (2015) 159–177, [1410.3012].

[65] S. Jadach, J. H. Kuhn, and Z. Was, *TAUOLA: A Library of Monte Carlo programs to simulate decays of polarized tau leptons,* Comput. Phys. Commun. **64** (1990) 275–299.

[66] **Belle II**, W. Altmannshofer et al., *The Belle II Physics Book,* PTEP **2019** (2019), no. 12 123C01, [1808.10567]. [Erratum: PTEP 2020, 029201 (2020)].

[67] **Belle II**, "Kaon and pion identification performances in Phase III data." BELLE2-NOTE-PL-2020-014, 2020.

[68] **Belle II**, "Measurement of the tracking efficiency and fake rate with $e^+ e^- → \tau^+ \tau^-$ events." BELLE2-NOTE-PL-2020-014, 2020.

[69] **Belle II Tracking Group**, V. Bertacchi et al., *Track finding at Belle II,* Comput. Phys. Commun. **259** (2021) 107610, [2003.12466].

[70] G. Punzi, *Sensitivity of searches for new signals and its optimization,* eConf **C030908** (2003) MODT002, [physics/0308063].

[71] P. Virtanen, R. Gommers, T. E. Oliphant, M. Haberland, T. Reddy, et al., *SciPy 1.0: Fundamental Algorithms for Scientific Computing in Python,* Nature Methods **17** (2020) 261–272.

[72] W. Baldini et al., *SHADOWS (Search for Hidden And Dark Objects With the SPS),* 2110.08025.